# Chapter 3

## T-Cell Proliferation Control with Ribozyme-Based Regulatory Systems

Adapted with permission from Chen, Y.Y., Jensen, M.C., & Smolke, C.D. Genetic control of mammalian T-cell proliferation with synthetic RNA regulatory systems. *Proc Natl Acad Sci USA* **107**, 8531-8536 (2010).

**Abstract**

RNA molecules perform diverse regulatory functions in natural biological systems, and numerous synthetic RNA-based control devices that integrate sensing and gene-regulatory functions have been demonstrated, predominantly in bacteria and yeast. Despite potential advantages of RNA-based genetic control strategies in clinical applications, there has been limited success in extending engineered RNA devices to mammalian gene expression control and no example of their application to functional response regulation in mammalian systems. Here, we describe a synthetic RNA-based regulatory system and its application in advancing cellular therapies by linking rationally designed, drug-responsive, ribozyme-based regulatory devices to the proliferative cytokines interleukin-2 (IL-2) and interleukin-15 (IL-15) to control mouse T-cell proliferation. We report the development of regulatory devices responsive to the small-molecule drugs theophylline and tetracycline, and demonstrate the ability of the regulatory devices to reversibly modulate target-gene expression levels within 12 hours of drug addition. We further demonstrate the ability of our synthetic controllers to effectively modulate *in vivo* T-cell expansion, achieving a 40% increase in T-cell growth rate in response to theophylline administration. Our RNA-based regulatory system exhibits unique properties critical for translation to therapeutic applications, including adaptability to diverse ligand inputs and regulatory targets, tunable regulatory stringency, and rapid response to input availability. By providing tight gene expression control with customizable ligand inputs, RNA-based regulatory systems can greatly improve cellular therapies and advance broad applications in health and medicine.

## Introduction

The ability to control functional responses in mammalian cells with customizable and compact regulatory systems *in vivo* addresses a critical need in diverse clinical applications, particularly in cellular therapies[1, 2]. As an example, adoptive T-cell therapy seeks to harness the precision and efficacy of the immune system against diseases that escape the body's natural surveillance. The adoptive transfer of antigen-specific T cells can reconstitute immunity to viruses and mediate tumor regression[3, 4], and early-stage clinical trials have demonstrated the potential of engineered T cells against cancer[5]. T cells engineered to express tumor-specific T-cell antigen receptors can achieve highly refined target recognition[6, 7], thus minimizing toxic off-target effects associated with conventional chemotherapy. However, considerable research has shown that the persistence of transferred T cells *in vivo* is both central to therapeutic success and elusive to current technology[8, 9]. The efficacy of adoptive immunotherapy in humans is often limited by the failure of transferred T cells to survive in the host[10-12].

Clonal expansion of T cells is a critical component of T-cell activation mediated by cytokines such as interleukin-2 (IL-2) and interleukin-15 (IL-15), which activate JAK-STAT signaling pathways and lead to the expression of genes involved in growth modulation[13]. Sustaining the survival and proliferation of T cells following adoptive transfer is challenging due to the limited availability of homeostatic cytokines (IL-15/IL-7) and stimulatory antigen presenting cells. State-of-the-art strategies for improving the persistence of adoptively transferred lymphocytes require that patients be subjected to myeloablative total body irradiation/chemotherapy and toxic levels of IL-2[14]. Alternative strategies based on the unregulated expression of growth-related genes pose the risk of

uncontrolled lymphoproliferation and leukemic transformation[8]. Thus, the ability to integrate growth stimulatory gene expression with tightly controlled regulatory systems has the potential to greatly improve the safety and efficacy of adoptive T-cell therapy.

As described in Chapter 1, numerous synthetic RNA-based regulatory systems have been developed. However, despite recent advances in the design of RNA devices that process and transmit specified molecular inputs to regulated gene expression events[15, 16], the absence of successful adaptations of these earlier genetic devices to the regulation of functional responses in mammalian cells highlights remaining difficulties in translating designs that regulate reporter gene expression to functional control. Here, we report a synthetic, small-molecule-responsive RNA-based gene regulatory system in mammalian cells and demonstrate its application in advancing cell-based therapies through the control of cell-fate decisions. We develop a genetic strategy for effectively controlling T-cell expansion based on drug-responsive RNA regulators that exert tight control over key upstream signaling molecules in the proliferation pathway. Our work demonstrates an RNA-based regulatory system that exhibits unique properties critical for translation to therapeutic applications, including adaptability to diverse input molecules and genetic targets, tunable regulatory stringency, and rapid input response.

## Results

**An RNA-Based System Enables Gene Expression and Viability Control in T Cells.** We developed an RNA-based regulatory system for mammalian T-cell proliferation based on a platform for assembling RNA devices from modular sensor (aptamer) and gene-regulatory (hammerhead ribozyme) components. The activity of this ribozyme

switch platform had been shown in the microorganism *Saccharomyces cerevisiae*[17, 18], and its ability to regulate gene expression in mammalian cells has been confirmed in human embryonic kidney (HEK) cells (see Chapter 2). However, the ability of ribozyme switch devices to regulate functional outputs in mammalian cells remains to be demonstrated.

Cytokines are potent growth-stimulatory molecules whose effects on cell growth are amplified through the JAK-STAT signaling pathway (Figure 3.1A). The ability to regulate upstream pathway molecules and take advantage of signal amplification through an endogenous pathway toward downstream functional responses is an important design strategy supported by our RNA regulatory system. We developed a cell-intrinsic control system for cytokine production based on ribozyme ON switches, which are RNA devices that convert a small-molecule input to an increased gene expression output (Figure 3.1B). The system design ensures suppression of cell growth as a default state and induction of cell proliferation only in the presence of an administered small-molecule drug input. In this system, the ribozyme-based device is placed in the 3' untranslated region (UTR) of a target transgene encoding a proliferative cytokine, where self-cleavage by the ribozyme results in rapid degradation of the target transcript and decreased cytokine production. The ribozyme device is designed to adopt at least two conformations (input-unbound and input-bound) associated with either a ribozyme-active or -inactive state. The presence of drug input stabilizes the input-bound, ribozyme-inactive conformation, thereby preserving transcript integrity and upregulating cytokine production, resulting in autocrine cell growth. The absence of drug input stabilizes the ribozyme-active

conformation, resulting in transcript degradation, reduced cytokine production, and diminished cell growth.

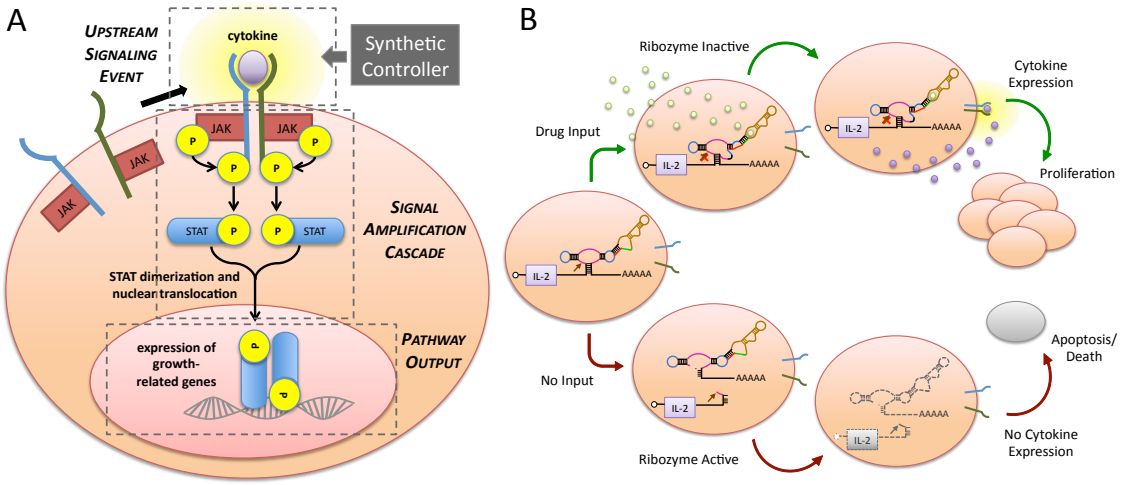


**Figure 3.1.** An engineered T-cell proliferation regulatory system utilizing a synthetic RNA device to achieve drug-mediated modulation of cell signaling and proliferation. (A) The common γ-chain T-cell proliferation pathway and integration of a synthetic controller targeted to the upstream signaling events. (B) An engineered T-cell proliferation regulatory system based on the programmable drug-mediated regulation of cytokine expression from a synthetic ribozyme switch. Ribozyme color scheme is as described in Ref. 17.

As a model system, a fusion transgene encoding a proliferative cytokine (IL-2) and a quantifiable protein marker (EGFP) served as the regulatory target to permit simultaneous quantification of the regulatory system's performance at the levels of direct gene expression (fluorescence) and downstream pathway output (viability) (Figure 3.2A). The cytokine and reporter proteins were linked through a self-cleaving T2A peptide (see Supplementary Text 3.1 for sequence) to ensure that the ribozyme switch activity was equally effective on the linked target genes but that the proteins folded and functioned as independent molecules. Three theophylline-responsive ribozyme switches (L2bulge1, 8, and 9; see Chapter 2 Materials and Methods for sequences), which had been tuned through sequence modifications to exhibit different regulatory response properties[17], were inserted into the 3' UTR of the *egfp-t2a-il2* fusion gene. Instead of the more commonly

used cytomegalovirus (CMV) immediate early promoter, which has been shown by previous reports[19-21] and our own studies (see Supplementary Text 3.2) to be prone to suppression and silencing upon genomic integration, the elongation factor 1 alpha (EF1α) promoter was used to drive the expression of the target transgene and ribozyme switches. Plasmids incorporating this regulatory system were transiently transfected into the CTLL-2 mouse T-cell line which, like primary human T cells, is dependent on common γ-chain signaling for survival and proliferation[22]. Each of the ribozyme switches resulted in input-responsive regulation over cell viability and fluorescence (Figure 3.2B, Supplementary Figure 3.1A; see Supplementary Text 3.3 for discussion on controls and normalization methods), confirming the prescribed function of these devices in mammalian cells. The ribozyme-based regulatory systems provided titratable response over a range of input concentrations (Figure 3.2C, Supplementary Figure 3.1B), demonstrating the ability to adjust expression levels based on input availability.

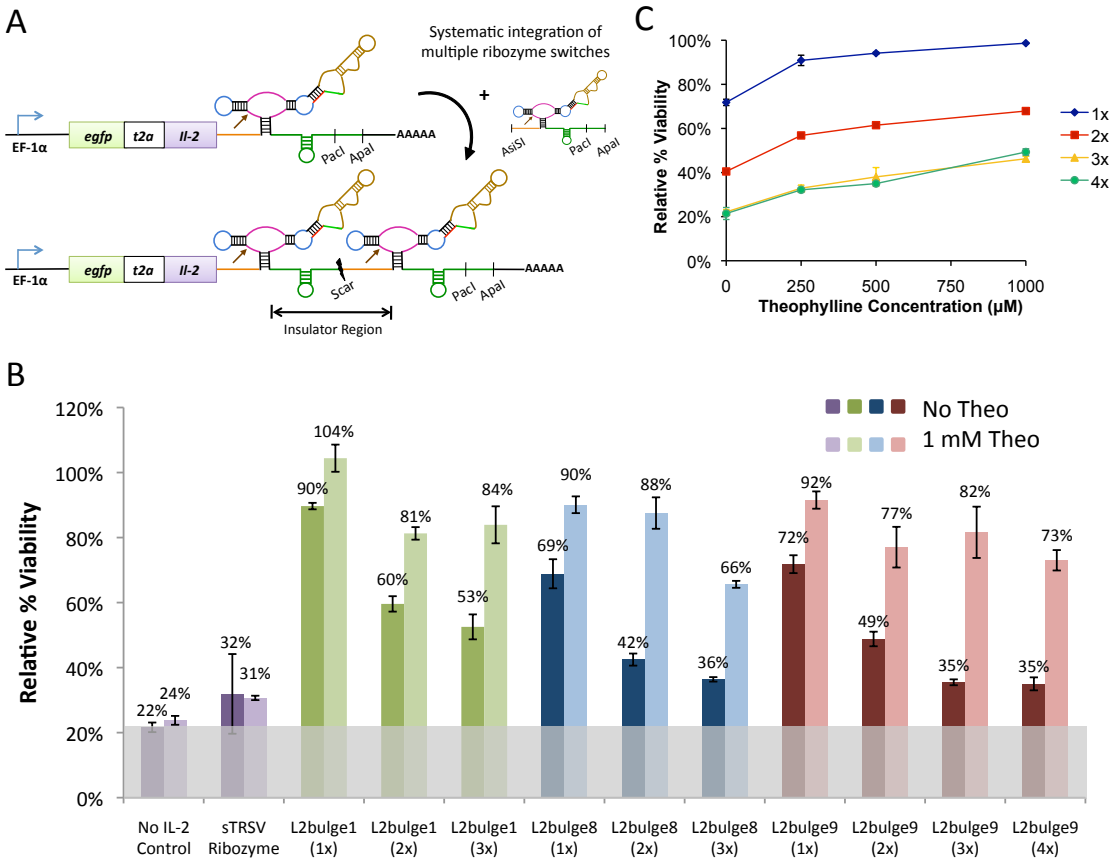


**Figure 3.2.** Modularly constructed ribozyme switches exhibit tunable, drug-mediated regulation of gene expression and cell growth in mammalian T cells. (A) A modular insertion strategy allows the implementation of multiple copies of ribozyme switches to tune regulatory stringency. Spacer sequences (orange, green) provide structural insulation and maintain the functional independence of each switch. (B) Ribozyme switches provide tunable, small-molecule-mediated regulatory systems. Cell viability levels are reported for constructs encoding theophylline-responsive switches (L2bulge1, 8, 9) in one (1x), two (2x), three (3x), and four (4x) copies through transient transfections in CTLL-2 cells grown in 0 and 1 mM theophylline. No IL-2 Control, construct not encoding a proliferative cytokine; sTRSV Ribozyme, construct encoding a non-switch hammerhead ribozyme. Gray bar indicates background viability level of cells in the absence of cytokine. (C) Ribozyme switches provide titratable regulatory systems. Cell viability levels are reported for the L2bulge9 regulatory systems at various theophylline concentrations. All values were normalized to those of controls expressing the appropriate transgene regulated by an inactive ribozyme and cultured at corresponding theophylline concentrations. Reported values are mean ± s.d. from at least two replicate samples.

**A General Strategy for Tuning the Dynamic Range of Ribozyme Switches Allows for Modulation of T-Cell Proliferation Response.** The potency of the genetic targets in our T-cell regulatory system requires stringent control over basal cytokine expression levels, such that in the absence of input the engineered T cells exhibit proliferation levels

similar to cells growing in the absence of cytokine. To engineer a more stringent regulatory system, we implemented a second tuning strategy based on linking multiple copies of the ribozyme switches in the 3' UTR of the transgene. As demonstrated by studies performed in HEK 293 cells and described in Chapter 2, multiple-copy expression is expected to lower the basal expression level since only one of the switches needs to be in a ribozyme-active state to cleave and inactivate the transcript. We developed a construction strategy for sequentially inserting ribozyme switches in the 3' UTR of the transgene and insulated the switches through spacer sequences designed to maintain the structural integrity and functional independence of each switch (Figure 3.2A, see Chapter 2 Materials and Methods).

Characterization of the multiple-copy switch systems indicated that this tuning strategy effectively decreased basal expression levels (Figure 3.2B, Supplementary Figure 3.1A) and that the titratable response of the system was maintained (Figure 3.2C, Supplementary Figure 3.1B). Stringent knockdown was achieved with three and four copies of the tightest switch (L2bulge9, Figure 3.2B), which resulted in viability levels comparable to cells transfected with no cytokine or with the fully active, non-switch ribozyme (No IL-2 Control and sTRSV Ribozyme, respectively). Notably, the regulatory performance of the four-copy switch system was similar to that of the three-copy system (Figure 3.2B), indicating that three copies of the tightest switch were sufficient to approach the minimum possible viability levels. The data underscore the non-linear relationship between direct gene expression and functional pathway outputs from the system. Whereas absolute changes in gene expression (fluorescence) in response to drug input remain similar for constructs with varying copies of a ribozyme switch

(Supplementary Figure 3.1A), the absolute changes in pathway output (viability) increased substantially with ribozyme copy number (Figure 3.2B).

**Ribozyme Switches Can Be Programmed to Respond to Alternative Drug Molecules.** The ON-state expression levels of drug-responsive RNA regulatory systems can be limited by the toxicity and cell permeability of the input molecule[23]. However, an important property of the ribozyme-based regulatory system is that its component functions are modular and thus amenable to changes that support customization for diverse applications, such as reprogramming input responsiveness toward clinically usable pharmaceuticals. To verify this critical property of our prototype T-cell proliferation control system, we replaced the theophylline aptamer[24] with the tetracycline aptamer[25] to construct a tetracycline-responsive switch (L2bulge18tc, Figure 3.3A). *In vitro* assays indicated tetracycline-responsive ON switch activity in CTLL-2 cells (Figure 3.3B). The tetracycline-responsive systems demonstrated lower basal expression levels and increased dynamic ranges in response to lower input concentrations relative to the theophylline-responsive systems. The improved performance can be attributed to several factors, including structural differences between the aptamers resulting in less disruption from the tetracycline aptamer to the ribozyme's activity, higher affinity of the tetracycline aptamer for its ligand[26], and increased membrane permeability of tetracycline relative to theophylline resulting in a higher intracellular concentration of tetracycline under similar extracellular concentrations. Although tetracycline is not a clinically applicable drug input, the tetracycline switch system demonstrates the ability to improve regulatory stringency by incorporating aptamer sequences that cause minimal obstruction

to ribozyme cleavage in the absence of ligand input. Furthermore, the tetracycline switches highlight the ability to significantly increase the switch dynamic range by utilizing aptamers with higher binding affinities and applying input molecules that can be administered to higher intracellular concentrations.

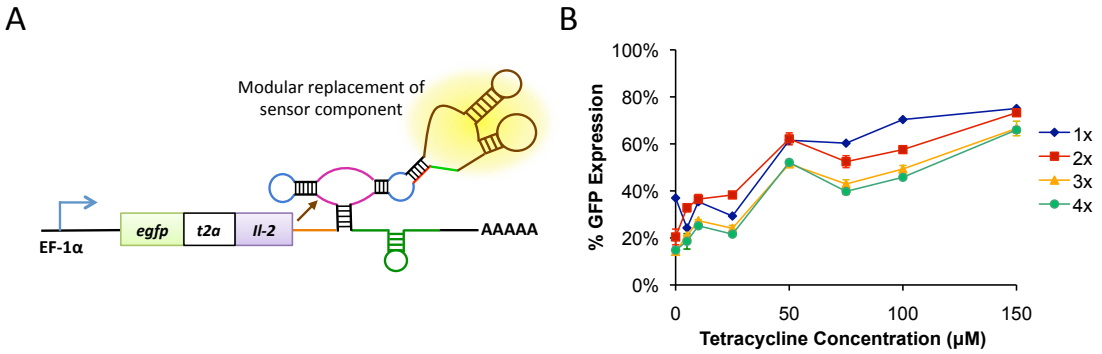


**Figure 3.3.** Ribozyme switches can be programmed to respond to alternative drug molecules. (A) Direct replacement of the sensor component allows tailoring of the input-responsiveness of the RNA-based regulatory system. (B) Reprogrammed device (L2bulge18tc) demonstrates titratable, tetracycline-responsive gene regulation. Values are reported as described in Figure 3.2, except control samples were cultured at corresponding tetracycline concentrations.

**A Clinically Relevant System Controls T-Cell Proliferation Based on Drug-Modulated Regulation of IL-15 Production.** Although IL-2 plays a critical role in the stimulation of activated T cells, it is also involved in activation-induced cell death (AICD) and the establishment of peripheral tolerance. Several studies have indicated that an alternative γ-chain cytokine, IL-15, provides potent homeostatic T-cell survival/proliferative signals, inhibits IL-2-mediated AICD, and may be superior to IL-2 in immunotherapy applications[27, 28]. Recently, IL-15 has been shown to function in establishing the long-term persistence of adoptively transferred central memory T ($T_{CM}$) cells in primates, suggesting significant potential in T-cell therapy for cancer[29]. To develop a more clinically relevant regulatory system, we utilized the modularity of the

ribozyme switch platform and replaced the *egfp-t2a-il2* transgene with a trifunctional fusion transgene (*cd19-tk-t2a-il15*) encoding IL-15, mutant HSV-1 thymidine kinase (ser39TK, a protein marker that can act as a PET reporter and as a suicide protein in the presence of the drug ganciclovir, providing imaging and safety kill-switch functionalities for downstream clinical implementations), and CD19 (a quantifiable protein marker amenable to FACS- and immunomagnetic-based selections). The alternative transgene was placed directly into the theophylline-responsive switch systems based on L2bulge9 (Figure 3.4A). Ribozyme switch systems with the altered target transgene exhibited ON-switch control over cell viability and proliferation in transient transfection experiments (Figure 3.4B), confirming modular coupling between the target transgene and the regulatory device. Samples expressing IL-15 showed higher viability levels compared to those expressing IL-2 with the corresponding switch systems (Figures 3.2C, 3.4B), suggesting IL-15 may be a more potent survival/proliferative cytokine and can better amplify the signal response. Therefore, under a low basal expression level, a small increase in IL-15 expression has the potential to significantly elevate the T-cell proliferation level.

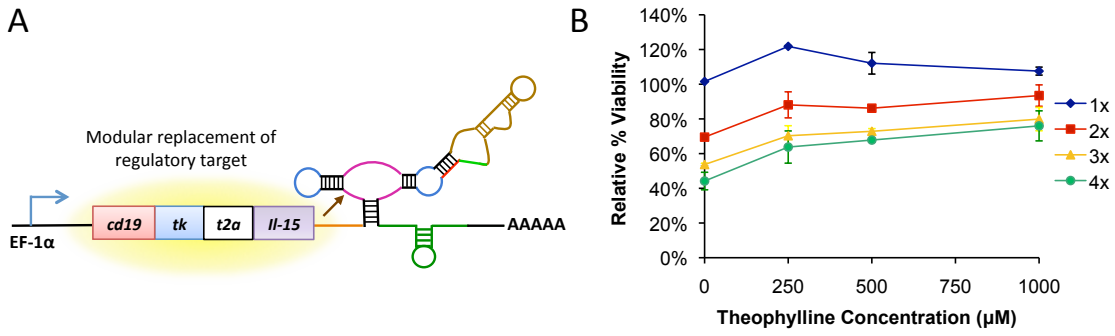


**Figure 3.4.** Ribozyme switches can be programmed to regulate alternative gene targets. (A) Direct replacement of the target gene allows tailoring of the output of the RNA-based regulatory system. (B) Reprogrammed system with the alternative regulatory target *cd19-tk-t2a-il15* achieves enhanced survival response compared to IL-2-based systems. Values are reported as described in Figure 3.2.

**Ribozyme Switches Enable Long-Term, Dynamic Control over Gene Expression.** To characterize long-term behavior of the regulatory system, we generated stable T-cell lines expressing the theophylline-responsive ribozyme switch systems. We generated a CTLL-2 cell line (CffLuc) that stably expressed the firefly luciferase (*ffluc*) gene to enable biophotonic imaging of cell populations *in vivo*. We subsequently integrated T-cell proliferation regulatory systems based on one or three copies of L2bulge9 into CffLuc. Stable integrants were initially sorted based on CD19 expression. At the bulk population level, cells stably expressing three copies of the ribozyme switch had a lower basal level and larger switch dynamic range in response to theophylline addition compared to cells stably expressing one copy of the ribozyme switch, consistent with transient transfection results (Supplementary Figure 3.2). We further refined the sorted population by alternating treatment with ganciclovir and IL-2 or with theophylline and no IL-2 (Figure 3.5) to enrich for clones with low basal expression levels and sufficiently high ON-state expression levels to sustain cell survival, respectively. We generated clonal cell lines by a final sorting step for CD19 positive cells in the presence of theophylline.

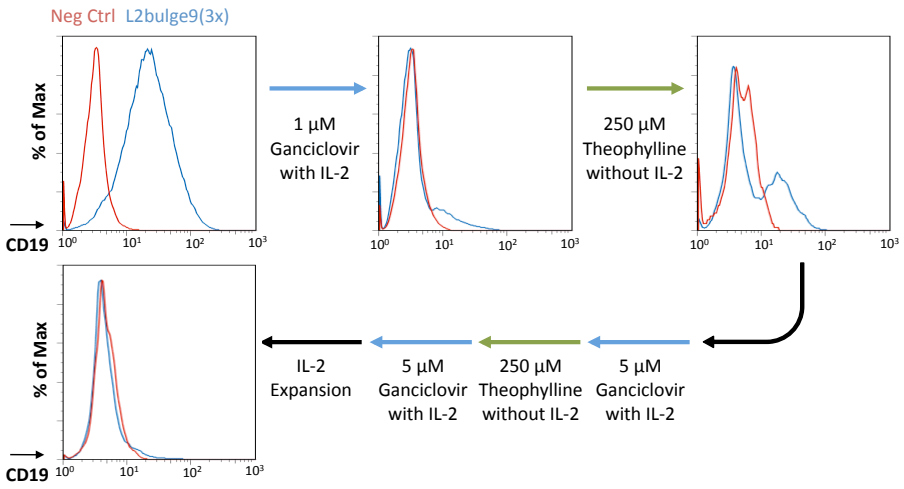


**Figure 3.5.** The generation of T-cell lines stably expressing ribozyme switch systems through alternate cycles of negative and positive selections. CTLL-2 cells stably expressing a luciferase reporter (CffLuc) were transfected with linearized plasmids encoding ribozyme switch systems based on L2bulge9. Stable integrants were initially sorted for CD19 expression and subsequently subjected to alternate cycles of negative and positive growth selection with ganciclovir and theophylline, respectively. Gene expression levels were monitored by staining with PE-conjugated CD19 antibodies; blue, bulk stable *cd19-tk-t2a-il15*-L2bulge9(3x) cell line; red, CffLuc cell line.

Growth behavior of individual clones was characterized by culturing under various theophylline concentrations. Results indicate that the T-cell proliferation regulatory system retained functionality over long time periods when stably integrated, and that theophylline effectively replaced IL-2 as the trigger for cell proliferation (Figure 3.6A). Fifteen of the sixteen clones examined showed substantial theophylline-responsive increase in cell growth (Supplementary Figure 3.3), supporting that the growth modulation effect is specific to the introduced regulatory system.

Additional assays on a clonal cell line harboring three copies of L2bulge9 (clone 1264-48) were performed to verify the mechanism of growth regulation and examine the dynamic behavior of the regulatory system to variations in theophylline availability. Cell cultures were grown for one week in the presence of 500 µM theophylline and continued for a second week in the absence of theophylline. Theophylline was reintroduced for

another four days at the end of the study. Compared to the identical clone continuously cultured in the absence of theophylline, the cell population exhibited elevated CD19 protein levels within 24 hours of theophylline addition and levels remained elevated throughout the period of theophylline treatment (Figure 3.6B). CD19 expression returned to basal levels within 48 hours of theophylline removal. The theophylline-responsive increase in CD19 expression was repeated upon reintroduction of theophylline to culture media. To determine a more precise time scale at which gene expression elevation occurs, the time course study was repeated with multiple time points taken within 48 hours of theophylline addition. Results indicate that the ribozyme-based system generates a regulatory response at the protein level within 12 hours of drug input addition (Figure 3.6C). IL-15 expression patterns were verified at the transcript level through qRT-PCR (Supplementary Figure 3.4A). Interestingly, the IL-15 protein levels as measured by intracellular antibody staining showed no response to drug input and no difference between cell lines expressing the inactive ribozyme control and the L2bulge9 switch construct despite clear differences in IL-15 mRNA and CD19 protein levels (Supplementary Figure 3.4B). Since CTLL-2 cells continuously export IL-15 in high flux, the signals detected by intracellular staining may indicate the steady-state protein level and thus show no difference among the cell lines and conditions tested. Finally, western blot analysis of phosphorylated STAT5 levels verified activation of the IL-15 receptor-signaling cascade in the presence of theophylline (Supplementary Figure 3.4C). These results highlight the ability of the ribozyme switch system to quickly, effectively, and robustly switch gene expression on and off in response to drug input.

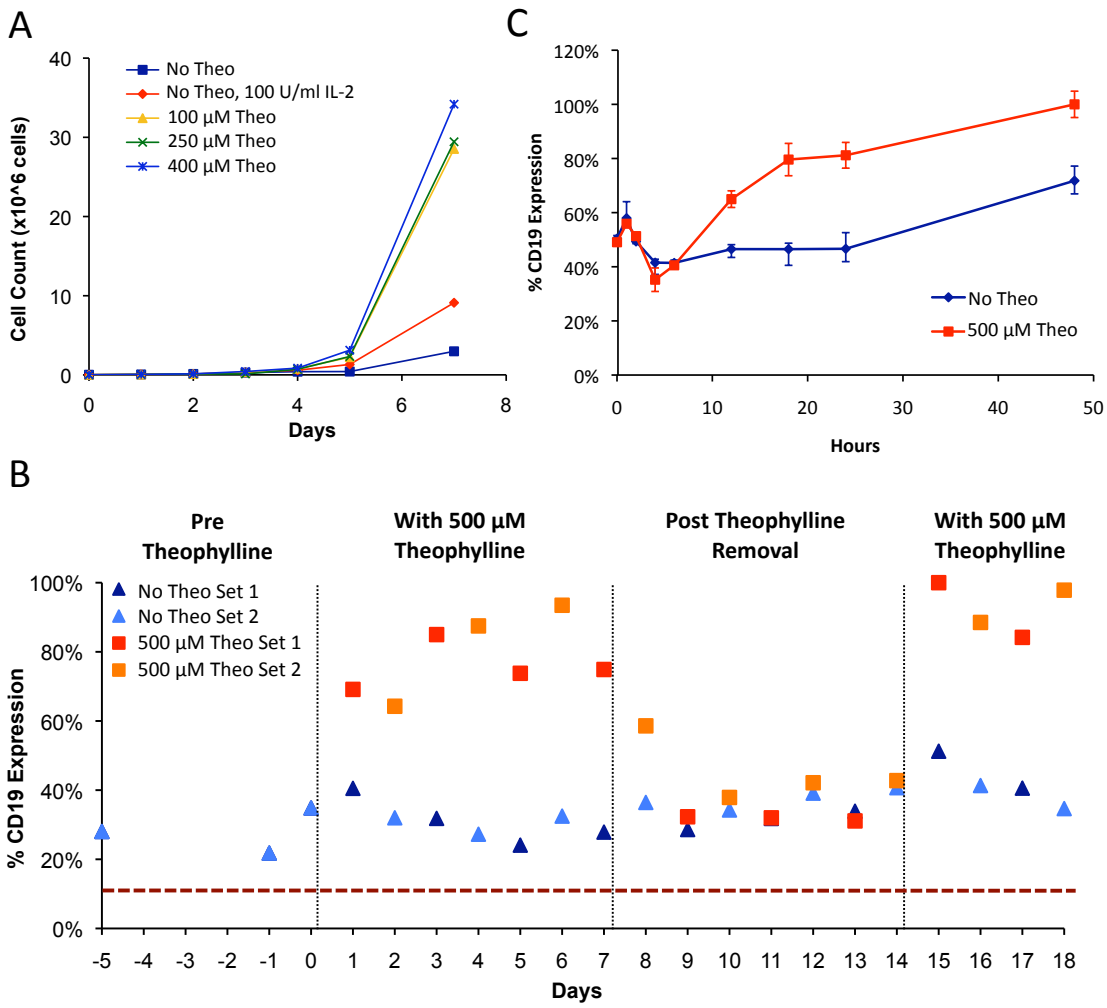


**Figure 3.6.** T cells stably expressing ribozyme switch systems exhibit drug-mediated regulation of growth over extended time periods *in vitro*. (A) Clonal cell lines stably expressing the ribozyme switch system exhibit drug-mediated growth. Cell growth was monitored by counting viable cells, and data for a representative clone (1264-48, expressing *cd19-tk-t2a-il15*-L2bulge9(3x)) are shown. (B) The ribozyme switch system regulates gene expression in response to changes in input concentrations. Duplicate sets of the clonal cell line 1264-48 were cultured in the presence (red and orange) and absence (light blue and dark blue) of theophylline over 18 days. Expression levels were monitored by staining with PE-conjugated CD19 antibodies, and values were normalized to those from the inactive ribozyme control. The highest expression level was set to 100%. Red dashed line indicates background-staining level of a cell line without a CD19 construct. (C) The ribozyme switch system generates regulatory response within 12 hours of input addition. Duplicate cultures were maintained in the presence (red) and absence (blue) of theophylline for 48 hours. Fluorescence values were obtained and normalized as in (B).

**Ribozyme Switches Enable Drug-Modulated Control over T-Cell Proliferation *In Vivo*.** To verify *in vivo* functionality of the T-cell proliferation regulatory system, we examined several clonal cell lines for theophylline-dependent growth in mice. Select

clones were encased in a hydrogel matrix that contained either 0 or 500 μM theophylline and injected into the flanks of NOD/SCID-$\gamma_c^{-/-}$ mice. Cell lines lacking the transgene regulatory system or stably expressing the inactive ribozyme construct served as negative and positive controls, respectively. *In vivo* T-cell expansion was not observed from clones lacking cytokine expression (No IL-15 control, Figure 3.7A), demonstrating the need for cytokine expression in sustaining cell growth. Uncontrolled T-cell proliferation was observed in the absence of a functional ribozyme-based regulatory device regardless of theophylline availability (Inactive Rz control, Figure 3.7A). In contrast, the clonal cell line 1264-48, which harbors three copies of L2bulge9, showed a significantly stronger reporter signal at the conclusion of the 14-day study when injected with 500 μM theophylline compared to the same clone injected without theophylline (L2bulge9(3x), Figure 3.7A). Growth rate calculations based on flux measurements over the 14-day period indicated a 32% increase in *in vivo* growth rate in the presence of 500 μM theophylline, leading to a 14-fold increase in luciferase signal (Figure 3.7B, Supplementary Figure 3.5). The *in vivo* study was repeated for clone 1264-48 with replicates, with the inactive ribozyme serving as the positive control. Flux measurements over a 9-day period indicated an average of 40% increase in the growth rate of clone 1264-48 in the presence of 500 μM theophylline ($n_1$ = 4, $n_2$ = 6, $P$ = 0.038 by Mann-Whitney U test). In contrast, the positive control did not show statistically significant changes in growth rate ($n_1$ = 6, $n_2$ = 6, $P$ = 0.394; Figure 3.7C, Supplementary Figure 3.6), indicating that the input-responsive growth behavior observed in clone 1264-48 was not due to non-specific effects of theophylline.

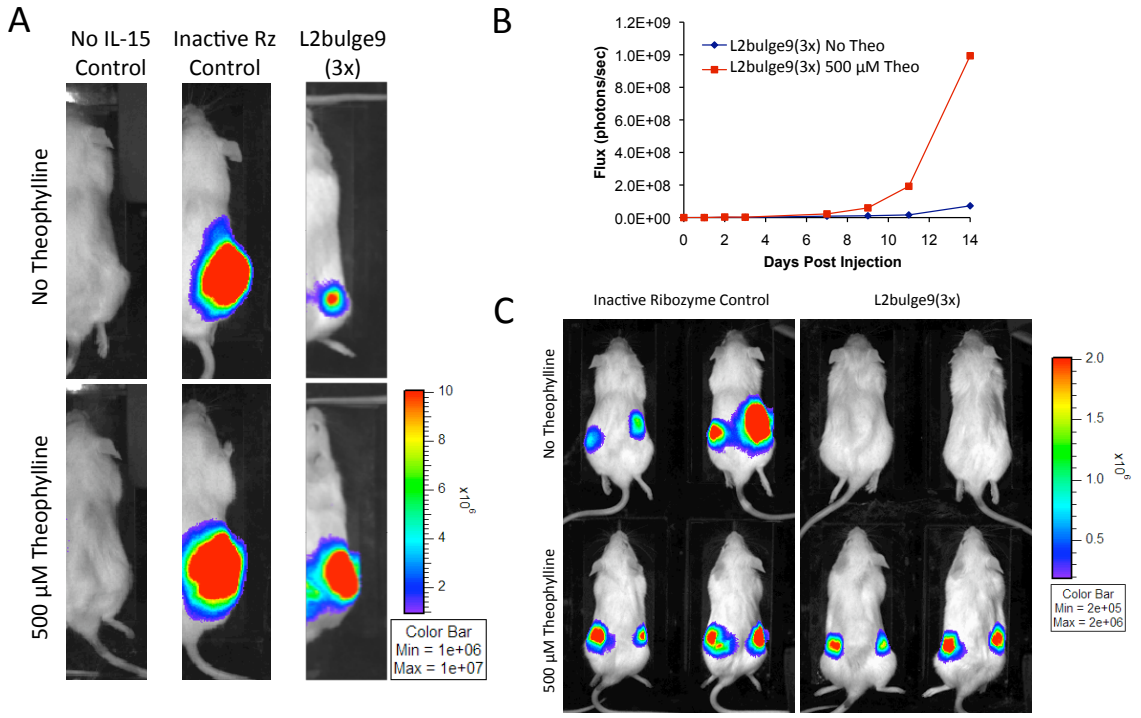


**Figure 3.7.** T cells stably expressing the ribozyme switch systems exhibit drug-mediated regulation of growth over extended time periods *in vivo*. (A) Both cytokine expression and functional ribozyme switches are required for effective regulation of T-cell proliferation. Images are shown for day 14 after injection of the negative control (No IL-15 Control, CffLuc), positive control (Inactive Rz Control, stable cell line expressing inactive ribozyme), and stable cell line expressing the ribozyme switch system (L2bulge9(3x), clone 1264-48) in the presence and absence of 500 µM theophylline. (B) Total luciferase signal flux over 14 days after injection of T cells is reported from the negative control (CffLuc) and clone 1264-48 (L2bulge9(3x)). (C) The ribozyme switch system demonstrates robust and reproducible small-molecule-mediated control over T-cell proliferation *in vivo*. Images are shown for day 4 after injection of the positive control and clone 1264-48. Identical clones were injected into the two flanks of each mouse in the presence or absence of 500 µM theophylline.

## Discussion

Achieving robust, controlled, long-term persistence of transfused T cells *in vivo* is a critical objective in adoptive immunotherapy, where efficacy depends on prolonged T-cell survival and safety demands stringent growth regulation. The T-cell proliferation challenge highlights a broader need for programmable regulatory systems that can modulate functional responses in mammalian cells. While numerous gene-regulatory systems have been developed, successful translation to clinical settings has been limited.

For example, synthetic inducible promoters rely on various transcriptional regulatory proteins, thus requiring multiple vectors and transgene expression systems. However, the stable expression of multiple transgenes in primary cell lines presents a significant challenge. In addition, concerns for potential immunogenicity of heterologous proteins limits the use of inducible promoters in clinical settings. Finally, the input specificity and regulatory dynamic range of such protein-based systems are relatively difficult to reprogram, thus limiting the flexibility and broader application of these system.

An alternative technology that has been pursued in the context of hematopoietic cell growth regulation is based on chemical inducers of dimerization (CIDs), which induce dimerization of pathway components fused to CID-binding domains[30-32]. However, studies conducted with CID-based systems have required lethally irradiated animal subjects to allow the expansion of transfused T cells with the assistance of homeostatic proliferation. In addition, several properties of the CID-based system hinder its broader application. For example, the system is limited to the regulation of homodimerization events, a mechanism that does not apply to many pathways of interest, including the common γ-chain signaling pathway central to T-cell persistence. The CID-based system is also fixed with respect to the input molecule, which is not available as a pharmaceutical drug.

Our synthetic, drug-responsive RNA-based regulatory system features properties that address critical limitations in existing genetic control strategies for clinical applications, including encapsulation within a compact, RNA-only platform (to avoid the use of immunogenic protein-based components) and allowing direct replacement of sensor and target transgene components (to tailor the technology to diverse applications).

This work presents the successful translation of an RNA device to the regulation of a functional response in mammalian cells. The unique capability to program the regulatory device's response properties was key to the effective transition from reporter gene expression regulation to functional control. By developing a rational tuning strategy for the regulatory stringency of our control system and integrating our synthetic controller with upstream signaling components, we were able to substantially enhance control over the functional system response. Furthermore, the observed non-linear relationship between direct gene expression levels and downstream pathway outputs highlights the importance of system design strategies. In particular, the ability to link synthetic controllers with relatively moderate gene regulatory activities to potent upstream pathway components enables dramatic alterations in downstream functional behaviors. The functional and structural independence of the ribozyme switch and its target gene enables the regulation of any transgene of interest and allows a high degree of flexibility in the design of optimal regulatory networks. Therefore, the identification of critical genetic components in a given system is both central to and readily accommodated by ribozyme switch-based regulation.

The unique modularity of our RNA-based device framework supports rapid and effective tailoring of the regulatory system to respond to clinically applicable inputs. Furthermore, the implementation of higher-order information processing devices[18] on platforms that integrate multiple aptamers to both endogenous and exogenous inputs will enable more sophisticated control strategies with applications in autonomous control systems, *in vivo* diagnosis, and precise localization of cellular therapeutics to disease targets. The development of RNA aptamers to pharmaceuticals with minimal off-target

toxicities and high cell permeability and bioavailability will be critical for the translation of these RNA-based regulatory systems to clinical applications. Therefore, the coupling of our modular device framework with advances in aptamer selection processes[33] will more broadly support the tailoring of RNA-based regulatory systems to diverse applications in health and medicine, including diagnostics, cellular therapeutics, gene therapy, and intelligent molecular therapies.

## Materials and Methods

**Plasmid construction.** All plasmids were constructed using standard molecular biology techniques[34]. Plasmid maps are provided in Supplementary Figure 3.7. All oligonucleotides were synthesized by Integrated DNA Technologies and all constructs were sequence verified (Laragen). Cloning enzymes, including restriction enzymes and T4 DNA ligase, were obtained from New England Biolabs and DNA polymerases were obtained from Stratagene.

A fusion of the firefly luciferase (*ffluc*) gene and the *Sh ble* gene encoding zeocin resistance was PCR amplified from pMOD-LucSh (Invivogen) using forward and reverse primers Kozak BamHI5' (5'ATCGGATCCGCCGCCACCATGGAGGATGCCAAGAA TATTAAGAAAGG) and zeocin XbaI3' (5'TATTCTAGATCAGTCCTGCTCCTCTGC CACAAAGTGC), respectively. The plasmid pffLuc:zeo was constructed by inserting the resulting PCR product into pcDNA3.1(+) (Invitrogen) via the unique restriction sites BamHI and XbaI located in the multi-cloning site behind the CMV promoter.

The *cd19* gene was PCR amplified from CD19t-Tk-T2A-IL15op_epHIV7 using forward and reverse primers CD19t BlpI5' (5'ATTGCTGAGCCTAGAGCTGAAG) and

CD19t-mutsr39TK FR (5'CCCGCAGTAGCGTGGGCATTCTTTTCCTCCTCAGGAC CAG), respectively. The thymidine kinase gene *mutsr39tk* was PCR amplified from mutsr39tk_pcDNA3.1(+) using forward and reverse primers CD19t-mutsr39TK FF (5'C TGGTCCTGAGGAGGAAAAGAATGCCCACGCTACTGCGGG) and mutsr39TK-T2A FR (5'CCTCTCCGCCGCCAGATCTGTTAGCCTCCCCCATCTCCC), respectively. The cytokine gene *il-15* was PCR amplified from CD19t-Tk-T2A-IL15op_epHIV7 using forward and reverse primers mutsr39TK FF (5'GGGAGATGGGGGAGGCTAACAGATCTGGCGGCGGAGAGG) and IL15op BsrGI3' (5'TCTCGGTGTACAGGGTGGCG), respectively. PCR products for the three genes were assembled via a fourth PCR reaction using forward and reverse primers CD19t BlpI5' and IL15op BsrGI3', respectively. The plasmid pIL15 was constructed by inserting the assembled PCR product (*cd19-mutsr39tk-t2a-il15*) into CD19t-Tk-T2A-IL15op_epHIV7 via the unique restriction sites BlpI and BsrGI behind the EF1α promoter.

The fluorescence gene *egfp* was PCR amplified from eGFP_pcDNA3.1(+) using forward and reverse primers eGFP KpnI5' (5'CTTGGTACCCGCCACCATGGTGAGC AAG) and T2A-IL2 FR (5'CCACGTCACCGCATGTTAGAAGACTTCCTCTGCCCTC TCCGCTGCCCTTGTACAGCTCGTCCATGCC), respectively. The cytokine gene *il-2* was PCR amplified from IL2_pSK using forward and reverse primers T2A-IL2 FF (5'CT TCTAACATGCGGTGACGTGGAGGAGAATCCCGGCCCTATGTACAGGATGCAA CTCCTGTC) and IL2 XhoI3' (5'AGACTCGAGTCAAGTTAGTGTTGAGATGATGC), respectively. PCR products for the two genes were assembled via a third PCR reaction using forward and reverse primers eGFP KpnI5' and IL2 XhoI3', respectively. The

plasmid eGFP-T2A-IL2_pcDNA3.1(+) was constructed by inserting the assembled PCR product (*egfp-t2a-il2*) into pcDNA3.1(+) via the unique restriction sites KpnI and XhoI behind the CMV promoter. A DNA sequence including the CMV promoter, the *egfp-t2a-il2* fusion gene, and the poly-A sequence was PCR amplified from eGFP-T2A-IL2_pcDNA3.1(+) using forward and reverse primers CMV HpaI5' (5'AATAGTTAACGTTGACATTGATTATTGACTAGTTATTAATAGTAATCAA) and bGHpA SacII3' (5'AATACCGCGGCCATAGAGCCCACCGC), respectively. The PCR product was inserted into dsRed Express_pcDNA3.1(+) via the unique restriction sites HpaI and SacII. The CMV promoter regulating the *egfp-t2a-il2* fusion gene was replaced by the EF1α promoter via the unique restriction sites BglII and KpnI to construct the plasmid pIL2. The EF1α promoter sequence was PCR amplified from pIL15 using forward and reverse primers EF1α BglII5' (5'AATAGATATCTGCTTCGCGA GGATCTGC) and EF1 α KpnI3' (5'AATAGGTACCGGTGGCGGCGCTAG), respectively. Multiple copies of ribozyme switches were inserted into the pIL2 and pIL15 vectors using sequential cloning methods described in Chapter 2.

**Mammalian cell culture maintenance.** The mouse T-cell line CTLL-2 was obtained from ATCC and maintained in RPMI-1640 media (Lonza) supplemented with 10% heat-inactivated fetal bovine serum (HI-FBS; Hyclone), 2 mM sodium pyruvate (Gibco), and 4.5 g/L D-(-)-glucose (Sigma). Cells were fed 100 U/ml IL-2 every 48 hours and maintained between 0.05 x $10^6$ and 0.50 x $10^6$ cells/ml. 0.20 mg/ml zeocin (Invivogen) was added to all cell lines stably expressing the ffLuc:zeocin fusion gene.

**Transient transfection and fluorescence quantification.** All transient transfections into CTLL-2 cells were performed with an Amaxa Nucleofector II and the Mouse T Cell Nucleofector Kit (Amaxa) following the manufacturer's protocols. Electroporations were performed with 2 x $10^6$ cells and 3 μg of plasmid DNA. One hour after electroporation, samples were diluted two-fold with supplemented RPMI media and split into 2 wells, one treated with small molecule input and one without input. In experiments testing a range of input concentrations, multiple aliquots of cells were electroporated as described. One hour after electroporation, samples were combined, diluted two-fold, split into the appropriate number of wells, and each treated with the appropriate concentration of small molecule input. Fluorescence and cell viability data were obtained 24 and 48 hours after transfection, respectively, using a Quanta Cell Lab Flow Cytometer (Beckman Coulter) equipped with a 488-nm laser. EGFP, PE, and dsRed-Express were measured through 525/30-nm band-pass, 575/30-nm band-pass, and 610-nm long-pass filters, respectively. Viability was gated based on side scatter and electronic volume, and only viable cells were included in fluorescence measurements. For samples expressing constructs based on pIL2, viable cells were further gated for dsRed-Express expression, which served as a transfection efficiency control, before EGFP intensity values were collected. All fluorescence measurements were reported as the geometric mean intensity observed in the gated population. To control for toxicity and other possible non-specific effects of transfection and input ligand molecules, cells transfected with an inactive (scrambled) hammerhead ribozyme and treated with the corresponding concentration of ligand molecule served as positive controls to which values from cells transfected with active ribozyme switches were normalized. The inactive ribozyme constructs provide controls

for the maximum possible gene expression levels from the ribozyme-based regulatory systems. CD19 antibody staining was performed by washing 1 x $10^6$ cells twice with 500 μl HBSS (Gibco), incubating with 10 μl PE-conjugated CD19 antibody (Beckman Coulter) in 50 μl HBSS for 15 min at 4°C in the dark, washing twice with 500 μl HBSS, and analyzing on the flow cytometer. Transient transfection experiments were performed with at least two replicate samples, and reported error bars indicate one standard deviation from the averaged measured value normalized by the inactive ribozyme control.

**Stable CTLL-2 cell line generation.** To generate a CTLL-2 cell line for *in vivo* imaging, CTLL-2 cells were electroporated with the pffLuc:zeo plasmid, and stable integrants were selected based on resistance to 0.1 mg/ml zeocin. The stable cell line CffLuc was confirmed through a luciferase activity assay, in which 1 x $10^4$ cells were resuspended in 100 μl media and aliquoted into 96-well black, clear-bottom plates. Each well was incubated with 20 μl of 1.4 mg/ml D-luciferin diluted in PBS (Xenogen) at 37°C for 10 min, and luciferase signal was detected using a Victor3 1420 Multilabel Counter (Perkin Elmer; Waltham, MA). Signals from six replicates were averaged for each experiment, and CTLL-2 cells not expressing *ffluc* were used as negative controls.

To generate CTLL-2 cells stably expressing constructs encoding the T-cell proliferation regulatory system for *in vivo* imaging, CffLuc cells were electroporated with plasmids derived from the pIL15 plasmid and linearized at the unique NsiI site. Electroporations for stable cell lines were carried out in seven cuvettes each containing 5 x $10^6$ cells and 5 μg plasmid DNA. One hour after electroporation, all electroporated samples were combined, diluted to a total volume of 50 ml, and supplemented with IL-2

every 48 hours to a final concentration of 100 U/ml. Cells were stained with PE-conjugated CD19 antibodies 7 days after electroporation and sorted for $PE^+$ cells by fluorescence-activated cell sorting (FACS) using a BD FACSAria cell sorter (BD Biosciences) equipped with a 488-nm laser. The sorted cells were grown for 13 days and then stained and further sorted via magnetism-automated cell sorting (MACS) using an autoMACS Separator (Miltenyi Biotec) for $PE^+$ cells. Theophylline was added to cell cultures to a final concentration of 250 μM 2 days prior to each sort.

Following the FACS and MACS sorts a series of selection cycles were performed by alternating between growth in ganciclovir and theophylline. Cells were grown for 2 weeks following AutoMACS sorting in media supplemented with IL-2 every 48 hours to a final concentration of 100 U/ml. The cells were then grown for 7 days in the presence of 1 μM ganciclovir and supplemented with IL-2 every 48 hours to a final concentration of 100 U/ml. The cells were subsequently placed in fresh media supplemented with 250 μM theophylline and allowed to grow for 4 days in the absence of IL-2. Following termination of theophylline treatment, the cells were placed in fresh media supplemented with 100 U/ml IL-2 (added every 48 hours) and 5 μM ganciclovir for 4 days. The theophylline treatment regime then resumed for 8 days, followed by the ganciclovir treatment regime (at 5 μM) for 10 days, and a final theophylline regime for 5 days. Cell density was maintained between $0.05 \times 10^6$ cells/ml and $0.5 \times 10^6$ cells/ml throughout the cell culture procedure. Following the last theophylline treatment regime, cells were stained with PE-conjugated CD19 antibodies and sorted for single clones into 96-well plates by FACS for low, medium, and high PE levels. The sorted clones (CffLuc-pIL15) were grown in media supplemented with 250 μM theophylline, 50 U/ml

penicillin:streptomycin, and no IL-2. Clones were expanded from the low PE fractions into larger culture volumes and finally maintained in T75 tissue culture flasks (BD Falcon).

***In vitro* growth assay for stable CTLL-2 cell lines.** CffLuc-pIL15 clones were cultured under regular conditions (RPMI 1640 media supplemented with 100 U/ml IL-2 every 48 hours, 0.2 mg/ml zeocin, no theophylline), washed twice with HBSS, and split into five identical aliquots in six-well plates at approximately 0.01 x $10^6$ cells/ml (4 ml/well). Each well was supplemented with one of the following: 100 U/ml IL-2, 100 μM theophylline, 250 μM theophylline, 400 μM theophylline, or no IL-2 and no theophylline. Cells were split and passaged as necessary into new six-well plates at approximately 0.03 x $10^6$ cells/ml, and IL-2 was added to the appropriate wells to a final concentration of 100 U/ml every 48 hours. Cell count was obtained from 50 μl of each culture daily for 7 days on a Quanta Cell Lab Flow Cytometer by gating for viable cells based on side scatter and electronic volume. Cell density was calculated by dividing the number of detected live cells by the volume analyzed on the flow cytometer.

**CTLL-2 time course study.** For the 18-day time course, CTLL-2 parental cells, clonal stable cell line 1264-48 (L2bulge9(3x)), and clonal stable cell line 1266-3 (inactive ribozyme) were cultured under regular conditions. On day 0, cells were counted for density and washed twice with HBSS. Each cell line was used to seed two 50-ml cultures at 0.15 x $10^6$ cells/ml (Set 1) and two 50-ml cultures at 0.05 x $10^6$ cells/ml (Set 2). 500 μM theophylline was added to one flask at each seeding density. 50 U/ml IL-2 was added

to Set 1 flasks and 100 U/ml IL-2 was added to Set 2 flasks to keep IL-2 concentration consistent with seeding cell density and harvesting schedule. On day 1, Set 1 flasks were harvested for CD19 antibody staining (1 x $10^6$ cells per sample) and for cell pellet collection for qRT-PCR (12.5 x $10^6$ cells per sample, washed once with HBSS, and flash frozen with liquid nitrogen). Each culture was split to 0.05 x $10^6$ cells/ml at 50 ml total and supplemented with 100 U/ml IL-2 and the appropriate concentration of theophylline (0 μM or 500 μM). On day 2, the same harvest and subculture procedures were repeated for Set 2 flasks. All cultures were treated in this manner every 48 hours until day 7. On day 7, cell count was obtained for all cultures. After harvesting from Set 1 flasks, all cultures were washed twice with HBSS and resuspended in fresh media without theophylline. Set 1 flasks were seeded at 0.05 x $10^6$ cells/ml and supplemented with 100 U/ml IL-2. Set 2 flasks were seeded with all available cells and supplemented with 50 U/ml IL-2. On days 8 and 9, the same harvest and subculture procedures were performed on Set 2 and Set 1 flasks, respectively. All cultures were treated in this manner every 48 hours until day 14. On day 14, cell count was obtained for all cultures. After harvesting from Set 2 flasks, all cultures were washed twice with HBSS and resuspended in fresh media. 500 μM theophylline was added to all cultures that had been treated with theophylline on days 0–7. Set 2 flasks were seeded at 0.05 x $10^6$ cells/ml and supplemented with 100 U/ml IL-2. Set 1 flasks were seeded with all available cells and supplemented with 50 U/ml IL-2. On days 15 and 16, samples were harvested for CD19 staining and subcultured as before for Set 2 and Set 1 flasks, respectively. All cultures were treated in this manner every 48 hours until day 18. For the 48-hour time course, CTLL-2 parental cells and the clonal stable cell line 1264-48 (L2bulge9(3x)) were

cultured under regular conditions. On day 0, cells were counted for density and washed twice with HBSS. Each cell line was used to seed four 30-ml cultures at 0.25 x $10^6$ cells/ml, each supplemented with 100 U/ml IL-2 and 50 U/ml penicillin streptomycin. 1.5 ml of each culture was sampled for surface staining with PE-CD19 antibody (0 hour time point), and theophylline was then added to two flasks of each cell line to a final concentration of 500 μM. Samples for antibody staining were taken at 1, 2, 4, 6, 12, 18, 24, and 48 hours after theophylline addition. Cultures were not fed with media, cytokine, or theophylline after the initial setup.

**Transcript analysis through qRT-PCR.** mRNA was purified from frozen cell pellets with the GenElute Direct mRNA MiniPrep Kit (Sigma) following the manufacturer's protocols. mRNA samples were treated with 100 U/ml DNaseI at 37°C for 15 min and purified by phenol-chloroform extraction and ethanol precipitation. Reverse transcription was performed with 300 ng mRNA, 2 pmol of each primer, 10 nmol dNTP, 40 U RNaseOUT, 5 mM DTT, 1x First-Strand Buffer, and 200 U SuperScript III Reverse Transcriptase (Invitrogen) in a 20 μl reaction following the manufacturer's protocols. Gene-specific primers (Hprt1 reverse, 5'TGCTGCCATTGTCGAACA; IL-15 reverse, 5'GGTGTCGTGGATGCTG) were used in the cDNA synthesis reactions. The resulting cDNA samples were subsequently treated with 2.5 U of RNaseH at 37°C for 20 min, followed by heat inactivation at 65°C for 20 min.

qRT-PCR reactions were performed in a 25 μl reaction with 200 nM of each primer, 5 μl cDNA, and 1x SYBR Green SuperMix (Bio-Rad) on an iCycler Real-Time PCR machine (Bio-Rad). Separate reactions were performed for the housekeeping gene

*Hprt1* (Hprt1 forward, 5'AGCCAGCGAAGCCAC; Hprt1 reverse) and the target gene *il-15* (IL-15 forward, 5'CAACTGGGTGAACGTGAT; IL-15 reverse). The qRT-PCR protocol included 32 cycles of a 15 sec annealing step at 50°C and a 30 sec extension step at 72°C, followed by a melt curve analysis to verify absence of non-specific products. All reactions were performed in triplicate, and threshold cycle ($C_t$) values were averaged to obtain the arithmetic mean. Relative IL-15 expression levels were calculated with the following formula [35]:

$$RE = \frac{\varepsilon_{Hprt1}^{(C_{t,Hprt1})}}{\varepsilon_{IL-15}^{(C_{t,IL-15})}}$$

where RE indicates relative IL-15 expression, $\varepsilon_x$ indicates primer efficiency for gene x, and $C_{t,x}$ indicates the averaged $C_t$ value for gene x. Standard deviation was calculated with the following formula:

$$STD = \sqrt{\left[RE\ln(\varepsilon_{Hprt1})\right]^2\left(Std_{Hprt1}\right)^2 + \left[RE\ln(\varepsilon_{IL-15})\right]^2\left(Std_{IL-15}\right)^2}$$

where STD indicates standard deviation in relative IL-15 expression and $Std_x$ indicates standard deviation calculated from the triplicate samples for gene x. Reported error bars indicate one standard deviation.

**Intracellular IL-15 antibody staining.** Approximately 1 x $10^6$ cells were harvested and washed once with 1 ml HBSS. The cell pellet was resuspended in 150 μl of BD Cytofix/Cytoperm buffer (BD Biosciences) and incubated on ice in the dark for 20 min. The sample was then washed twice with 1 ml of 1X BD Perm/Wash buffer and resuspended in 95 μl of 1X BD Perm/Wash buffer with 5 μl of anti-human IL-15-fluorescein monoclonal antibody (R&D Systems) and incubated on ice in the dark for 30

min. The sample was then washed twice with 1 ml of 1X BD Perm/Wash buffer, resuspended in 300 μl HBSS, and analyzed using a Quanta Cell Lab Flow Cytometer (Beckman Coulter) with excitation by a 488-nm laser and emission detected through a 525/30 band-pass filter.

**Western blot analysis of STAT5 levels.** Clonal stable cell lines were cultured under regular conditions (see above), washed twice with HBSS, and split into two identical aliquots. The aliquots were grown in the absence of IL-2 and either in the presence or absence of 500 μM theophylline for 3 days. Approximately 2 x $10^6$ cells of each sample were harvested and washed with 1 ml HBSS each day, frozen with liquid nitrogen, and stored at –80°C until lysis. Cell pellets were lysed with 50 μl Triton-X lysis buffer (1% Triton-X, 10 mM Tris-HCl, pH 7.4, 130 mM NaCl, 5 mM EDTA, protease inhibitor, 5% phosphatase inhibitor cocktail II) and incubated on ice for 1 hour. Lysates were centrifuged at 14,000 xg for 20 min at 4°C. The supernatant was collected and immediately frozen at –80°C.

Lysate samples were thawed on ice and a standard Bradford assay using Protein Assay Dye (Bio-Rad) was performed with a BSA standard to determine protein concentrations. Samples were run on NuPAGE 4-12% Bis-Tris Gels (Invitrogen) at 90 V for 2.5 hours, where 50 μg of protein from each sample was loaded. Blotting was performed with Mini Trans-Blot Filter Paper (Bio-Rad) and 0.45 μm Nitrocellulose Membranes (Bio-Rad) wetted with NuPAGE transfer buffer (Invitrogen) and transferred at 40 mA per gel with a Hoefer Semi-Phor Blotter (Hoefer Scientific Instruments). Membranes were blocked with Odyssey Blocking Buffer (Li-Cor) at 4°C for 1 hour and

probed with Rabbit-anti-pSTAT5 antibody (Cell Signaling) or IRDye 800CW-conjugated anti-β-actin antibody (Rockland) at 4°C overnight in the dark. Membranes probed with p-STAT5 antibodies were washed four times with 100 ml TTBS (1x Tris-Buffered Saline (TBS, Bio-RAD), 0.1% Tween 20 (Sigma)) and further stained with IRDye 800CW-conjugated goat-anti-rabbit antibody (Li-Cor) at room temperature for 1 hour. Membranes stained for β-actin and p-STAT5 were washed four times with 100 ml TTBS and once with 100 ml TBS before fluorescent images were acquired and quantified with the Odyssey Infrared Imaging System (Li-Cor). Integrated band intensity was calculated with the Odyssey system using blank gel areas surrounding each band for background subtraction. Relative p-STAT5 expression levels were calculated by normalizing the integrated intensity of the p-STAT5 band by that of the β-actin band from the same protein sample. Data shown are representative of two independent experiments.

***In vivo*** **T-cell proliferation studies in NOD/SCID-IL2(ko) mice.** Various CffLuc-pIL15 cell lines, CffLuc, and a CffLuc-derived cell line stably expressing a cytokine fusion transgene with an inactive ribozyme in the 3' UTR of the transgene were expanded under regular culture conditions. Cells were harvested by centrifugation at 1200 rpm at 4°C for 10 min, washed twice with PBS, resuspended in PBS at a concentration of 2 x $10^6$ cells/ml, and split into two 50 μl aliquots. Each aliquot was mixed with 50 μl of either PBS or 2 mM theophylline dissolved in PBS. The 100 μl cell suspension was then mixed with 100 μl of Matrigel (BD Biosciences), for a total of 0.1 x $10^6$ cells at a final concentration of 0 μM or 500 μM theophylline. The cell suspensions were injected subcutaneously (s.c.) into the right or left flank of NOD/scid-IL2(ko) mice. All mice were

8 to 10 weeks old and bred in the City of Hope lab animal breeding facility, and experiment protocols were approved by the City of Hope Institute Animal Care and Use Committee. *In vivo* growth of the injected cells was monitored by biophotonic imaging. Clone 1264-48 and the positive control cell line expressing an inactive ribozyme were tested in a second experiment following the procedure described above. Each cell line was injected into both flanks of three mice either with or without 500 μM theophylline, generating six replicates for each experimental condition. One of the mice injected with clone 1264-48 without theophylline exhibited abnormally large engraftments in both flanks. Additional subjects were studied to verify that cell growth in this mouse was aberrant in a statistically significant manner ($P = 0.044$ based on comparison against eight other replicates with the same experimental condition), and data from this mouse were excluded from statistical analyses of the ribozyme switch system.

**Biophotonic *in vivo* imaging.** Animals received intraperitoneal (i.p.) injections of 4.29 mg per mouse of freshly prepared luciferin substrate (Caliper Life Sciences) suspended in 150 μl of PBS. Mice were then anesthetized with isoflurane (1.5 L oxygen + 4% isoflurane per minute) in an induction chamber. After induction of deep anesthesia, mice were imaged using the IVIS Imaging System 100 Series (Xenogen) consisting of a CCD camera mounted on a light-tight specimen chamber (darkbox), a camera controller, a camera cooling system, and a Windows computer system for data acquisition and analysis. Images were acquired at 10–20 min after luciferin injection with the appropriate exposure time and binning mode to prevent signal saturation. Luciferase activity was

analyzed through Living Image Software 3.1 from Xenogen to quantify tumor region flux (photons per second).

**Statistical analysis.** Statistical analysis was performed on growth rate data using the Mann-Whitney U test to calculate two-tailed *P* values. The doubling time of injected cells was calculated based on the total luciferase signal flux data collected over the course of each *in vivo* study. Signal flux data were fitted to an exponential curve, and the resulting equation was used to calculate cell-doubling time using the equation:

$$t_D = (t_2 - t_1)\frac{\log(2)}{\log(F_2 - F_1)},$$

where t is time, F is signal flux, and $t_D$ is doubling time.

**Acknowledgments**

We thank members of the Smolke Lab, Y.A. Chen, and D. Endy for critical reading of the manuscript; M.N. Win for contributing expertise on ribozyme switch design; B. Aguilar, C. Bautista, C. Brown, L. Brown, W. Chang, R. Diamond, A. Hamlett, M. Hunter, D. Perez, G. Raval, J. Wagner, W. Wong, and C. Wright for technical assistance. This work was supported by the City of Hope's National Cancer Institute–Cancer Center Support Grant, the National Science Foundation (fellowship to Y.Y.C.), the Alfred P. Sloan Foundation (fellowship to C.D.S.), and the National Institutes of Health (grant to C.D.S., RC1GM091298).

**References**


1. Blattman, J.N. & Greenberg, P.D. Cancer immunotherapy: a treatment for the masses. *Science* **305**, 200-205 (2004).
2. June, C.H. Principles of adoptive T cell cancer therapy. *J Clin Invest* **117**, 1204-1212 (2007).
3. Falkenburg, J.H., Smit, W.M. & Willemze, R. Cytotoxic T-lymphocyte (CTL) responses against acute or chronic myeloid leukemia. *Immunol Rev* **157**, 223-230 (1997).
4. Walter, E.A. et al. Reconstitution of cellular immunity against cytomegalovirus in recipients of allogeneic bone marrow by transfer of T-cell clones from the donor. *N Engl J Med* **333**, 1038-1044 (1995).
5. Morgan, R.A. et al. Cancer regression in patients after transfer of genetically engineered lymphocytes. *Science* **314**, 126-129 (2006).
6. Gonzalez, S. et al. Genetic engineering of cytolytic T lymphocytes for adoptive T-cell therapy of neuroblastoma. *J Gene Med* **6**, 704-711 (2004).
7. Kahlon, K.S. et al. Specific recognition and killing of glioblastoma multiforme by interleukin 13-zetakine redirected cytolytic T cells. *Cancer Res* **64**, 9160-9166 (2004).
8. Leen, A.M., Rooney, C.M. & Foster, A.E. Improving T cell therapy for cancer. *Annu Rev Immunol* **25**, 243-265 (2007).
9. Robbins, P.F. et al. Cutting edge: persistence of transferred lymphocyte clonotypes correlates with cancer regression in patients receiving cell transfer therapy. *J Immunol* **173**, 7125-7130 (2004).

10. Dudley, M.E. et al. Adoptive transfer of cloned melanoma-reactive T lymphocytes for the treatment of patients with metastatic melanoma. *J Immunother* **24**, 363-373 (2001).

11. Yee, C. et al. Adoptive T cell therapy using antigen-specific CD8+ T cell clones for the treatment of patients with metastatic melanoma: in vivo persistence, migration, and antitumor effect of transferred T cells. *Proc Natl Acad Sci U S A* **99**, 16168-16173 (2002).

12. Mackensen, A. et al. Phase I study of adoptive T-cell therapy using antigen-specific CD8+ T cells for the treatment of patients with metastatic melanoma. *J Clin Oncol* **24**, 5060-5069 (2006).

13. Johnston, J.A. et al. Tyrosine phosphorylation and activation of STAT5, STAT3, and Janus kinases by interleukins 2 and 15. *Proc Natl Acad Sci U S A* **92**, 8705-8709 (1995).

14. Gattinoni, L., Powell, D.J., Jr., Rosenberg, S.A. & Restifo, N.P. Adoptive immunotherapy for cancer: building on success. *Nat Rev Immunol* **6**, 383-393 (2006).

15. Isaacs, F.J., Dwyer, D.J. & Collins, J.J. RNA synthetic biology. *Nat Biotechnol* **24**, 545-554 (2006).

16. Isaacs, F.J. et al. Engineered riboregulators enable post-transcriptional control of gene expression. *Nat Biotechnol* **22**, 841-847 (2004).

17. Win, M.N. & Smolke, C.D. A modular and extensible RNA-based gene-regulatory platform for engineering cellular function. *Proc Natl Acad Sci U S A* **104**, 14283-14288 (2007).

18. Win, M.N. & Smolke, C.D. Higher-order cellular information processing with synthetic RNA devices. *Science* **322**, 456-460 (2008).

19. Palmer, T.D., Rosman, G.J., Osborne, W.R. & Miller, A.D. Genetically modified skin fibroblasts persist long after transplantation but gradually inactivate introduced genes. *Proc Natl Acad Sci U S A* **88**, 1330-1334 (1991).

20. Choi, K.H., Basma, H., Singh, J. & Cheng, P.W. Activation of CMV promoter-controlled glycosyltransferase and beta-galactosidase glycogenes by butyrate, tricostatin A, and 5-aza-2'-deoxycytidine. *Glycoconj J* **22**, 63-69 (2005).

21. Xia, X., Zhang, Y., Zieth, C.R. & Zhang, S.C. Transgenes delivered by lentiviral vector are suppressed in human embryonic stem cells in a promoter-dependent manner. *Stem Cells Dev* **16**, 167-176 (2007).

22. Gillis, S. & Smith, K.A. Long term culture of tumour-specific cytotoxic T cells. *Nature* **268**, 154-156 (1977).

23. Beisel, C.L. & Smolke, C.D. Design principles for riboswitch function. *PLoS Comput Biol* **5**, e1000363 (2009).

24. Jenison, R.D., Gill, S.C., Pardi, A. & Polisky, B. High-resolution molecular discrimination by RNA. *Science* **263**, 1425-1429 (1994).

25. Berens, C., Thain, A. & Schroeder, R. A tetracycline-binding RNA aptamer. *Bioorg Med Chem* **9**, 2549-2556 (2001).

26. Weigand, J.E. & Suess, B. Tetracycline aptamer-controlled regulation of pre-mRNA splicing in yeast. *Nucleic Acids Res* **35**, 4179-4185 (2007).

27. Hsu, C. et al. Primary human T lymphocytes engineered with a codon-optimized IL-15 gene resist cytokine withdrawal-induced apoptosis and persist long-term in the absence of exogenous cytokine. *J Immunol* **175**, 7226-7234 (2005).

28. Waldmann, T.A., Dubois, S. & Tagaya, Y. Contrasting roles of IL-2 and IL-15 in the life and death of lymphocytes: implications for immunotherapy. *Immunity* **14**, 105-110 (2001).

29. Berger, C. et al. Adoptive transfer of effector CD8+ T cells derived from central memory cells establishes persistent T cell memory in primates. *J Clin Invest* **118**, 294-305 (2008).

30. Blau, C.A., Peterson, K.R., Drachman, J.G. & Spencer, D.M. A proliferation switch for genetically modified cells. *Proc Natl Acad Sci U S A* **94**, 3076-3081 (1997).

31. Neff, T. et al. Pharmacologically regulated in vivo selection in a large animal. *Blood* **100**, 2026-2031 (2002).

32. Zhao, S., Weinreich, M.A., Ihara, K., Richard, R.E. & Blau, C.A. In vivo selection of genetically modified erythroid cells using a jak2-based cell growth switch. *Mol Ther* **10**, 456-468 (2004).

33. Wilson, D.S. & Szostak, J.W. In vitro selection of functional nucleic acids. *Annu Rev Biochem* **68**, 611-647 (1999).

34. Sambrook, J. & Russell, D.W. Molecular Cloning: A Laboratory Manual, Edn. 3. (Cold Spring Harbor Press, Cold Spring Harbor; 2001).

35. Livak, K.J. & Schmittgen, T.D. Analysis of relative gene expression data using real-time quantitative PCR and the 2(-Delta Delta C(T)) Method. *Methods* **25**, 402-408 (2001).

**Supplementary Text 3.1**

**T2A Sequences**

*T2A DNA sequence*
GGCAGCGGAGAGGGCAGAGGAAGTCTTCTAACATGCGGTGACGTGGAGGAG
AATCCCGG

*T2A peptide sequence*
GSGEGRGSLLTCGDVEENPG

**Supplementary Text 3.2**

**CMV Promoter Silencing in Stably Integrated CTLL-2 Cells.** The CMV promoter is a powerful and frequently used driver of transgene expression in mammalian cells. Our initial system for implementing ribozyme-based regulatory devices in mammalian cells used the CMV promoter to express the target transgene coupled to ribozyme switches (Figure 2.3). To study the long-term performance of these regulatory systems in T cells, we stably integrated constructs encoding the *egfp-t2a-il2* transgene linked with one to four copies of the theophylline-responsive L2bulge9 switch into the genome of the CffLuc cell line. The results, discussed in detail below, suggest that the CMV promoter is easily silenced in stably integrated CTLL-2 cells and is unsuited for long-term expression of regulatory systems in this cell line.

In our initial ribozyme-based regulatory system design, one CMV promoter drove the expression of the *egfp-t2a-il2* transgene coupled to ribozyme switches, and a second CMV promoter drove the expression of *dsred-express*, which served as a transfection marker (Supplementary Figure 3.8). CffLuc cells were electroporated with DNA plasmids, selected for plasmid-encoded hygromycin resistance, and subjected to multiple rounds of population refinement by FACS. A cell line expressing *egfp-t2a-il2* coupled to

an inactive ribozyme was included as a positive control. Cultures were first sorted for dsRed$^+$ expression to isolate bulk populations with stable genomic integration on day 19 after electroporation (Supplementary Figure 3.9). Since the plasmid encodes for both EGFP and dsRed-Express, cells were expected to be either EGFP$^-$/dsRed$^-$ (double negative; no genomic integration) or EGFP$^+$/dsRed$^+$ (double positive; with genomic integration). Although varying degrees of EGFP knockdown were anticipated from the L2bulge9 constructs, all five cell lines, including the positive control, showed substantial single-positive populations that were either EGFP$^+$/dsRed$^-$ or EGFP$^-$/dsRed$^+$. These results suggest that a significant portion of the cells either integrated an incomplete fragment of the transfected plasmid, or at least one CMV promoter in the integrated construct had been silenced.

Bulk populations from the first sort were expanded in the presence of hygromycin and then cultured in the presence of 1 mM theophylline for six days prior to a second sort for dsRed$^+$/EGFP$^+$ populations on day 38 after electroporation (Supplementary Figure 3.10). This sorting scheme was designed to isolate bulk populations with high ON-state expression levels. Although the cells had previously been sorted for dsRed$^+$ expression and were cultured in the presence of hygromycin to ensure retention of the integrated transgenes, all four cell lines showed large dsRed$^-$ populations prior to the second sort, indicating that a substantial portion of the bulk population had lost expression from the CMV promoter.

The dsRed$^+$/EGFP$^+$ populations collected from the second sort were expanded in the presence of hygromycin. Cells harboring two and four copies of L2bulge9 were characterized for theophylline-responsive switch activities. Cultures were grown in the

presence of 0 mM, 0.5 mM, or 1 mM theophylline for 12 days, and EGFP expression was monitored by flow cytometry. Results indicate dose-dependent theophylline-responsive ON switch behavior from both the L2bulge9(2x) and the L2bulge9(4x) constructs starting within 24 hours of theophylline addition and continuing through the remainder the time-course experiment (Supplementary Figure 3.11).

To verify the regulation of functional output (i.e., cell proliferation) cells expressing L2bulge9(2x) and L2bulge9(4x) were characterized in mouse models. Cells expressing either no *egfp-t2a-il2* or the transgene coupled to an inactive ribozyme served as negative and positive controls, respectively. One million cells of each cell line were injected subcutaneously into the right flank of each of six mice. Three mice from each group subsequently received two systemic injections of 2.5 mg theophylline on the same day. One day after injections, six of the twelve mice that received theophylline were found dead, suggesting that the theophylline dosage used was too toxic for the animals. The remaining subjects were monitored by biophotonic imaging for ten days, and results indicate that all cell lines expressing *egfp-t2a-il2*, regardless of the ribozyme switch devices coupled to the transgene, were able to engraft *in vivo* (Supplementary Figure 3.12). Engrafted tumors were excised from the mice and analyzed by flow cytometry. Comparison of extracted tumor cells against the original cell lines continuously cultured *ex vivo* indicate that the animal hosts had exerted growth-based selection pressure on the injected cells and yielded a population with greatly elevated gene expression levels (Supplementary Figure 3.13). These results suggest that monoclonal cell populations with consistent and low OFF-state gene expression levels are required for effective growth regulation *in vivo*.

The L2bulge9(4x) bulk cell line was subsequently cultured in the absence of theophylline and sorted on day 109 after electroporation for single clones that were both $dsRed^{+}$ and either $EGFP^{-}$ or $EGFP^{low}$ to ensure low OFF-state expression levels (Supplementary Figure 3.14). The inactive ribozyme bulk cell line was sorted for single clones that were $dsRed^{+}/EGFP^{high}$ to provide a strong positive control. Despite the fact that the cells had been twice sorted for $dsRed^{+}$ expression and were continuously cultured in the presence of hygromycin, the majority of both cell lines fell in the double-negative quadrant during the third sort, indicating that CMV promoter silencing progressed as the cells remained in continuous culture.

Five clonal cell lines expressing L2bulge9(4x) were tested in mouse models with a clonal cell line expressing the inactive ribozyme serving as the positive control. CffLuc cells were also included as a negative control in the study. $0.1 \times 10^{6}$ cells of each cell line was injected subcutaneously into the right flank of a mouse, and cell proliferation was monitored by biophotonic imaging for 19 days. Results show that the positive control achieved robust engraftment while none of the L2bulge9(4x) cell lines expanded beyond background levels, indicating that the OFF-state expression levels were sufficiently low to avoid cell proliferation in the absence of theophylline (Supplementary Figure 3.15).

To test for theophylline-responsive switch behavior without using lethal doses of theophylline, $0.1 \times 10^{6}$ cells of each of five clonal L2bulge9(4x) cell lines were encased in a hydrogel matrix containing 200 μM theophylline and injected subcutaneously into the flanks of mice. The animals were monitored by biophotonic imaging for 15 days. By day 4 after injection, none of the L2bulge9(4x) cell lines showed engraftment (Supplementary Figure 3.16). Several of the animal subjects died prior to the end of the

experiment, but the cause of death is believed to be the general vulnerability of irradiated, immunosuppressant mice rather than the specific experimental conditions used. Based on the available data, none of the L2bulge9(4x) cell lines showed engraftment by day 8 after injection, suggesting that the cell lines either had lost the *egfp-t2a-il2* transgene or was unable to express the transgene at sufficiently high levels in the presence of 200 μM theophylline to sustain T-cell proliferation *in vivo*.

To verify that the *egfp-t2a-il2* transgene was still present in the genome, genomic DNA was extracted from each of the five L2bulge9(4x) clonal cell lines. The CffLuc cell line served as a negative control. Two positive controls were included: 1) a clonal cell line expressing *egfp-t2a-il2* coupled to the inactive ribozyme control and 2) a cell line expressing *egfp-t2a-il2* without any ribozyme device attached. PCR using a forward primer annealing to *egfp* and a reverse primer annealing to *il-2* was performed, and all cell lines other than the negative control showed the expected PCR product band, indicating that the *egfp-t2a-il2* transgene was stably integrated (Supplementary Figure 3.17A). Total RNA was extracted from each of the cell lines and qRT-PCR was performed using the forward and reverse primers mentioned above. L2bulge9(4x) Clone #4 showed no detectable signal while the other four L2bulge9(4x) clones showed less than 4% EGFP-T2A-IL2 expression relative to the inactive ribozyme, suggesting that the expression levels was likely too low to support T-cell proliferation *in vivo* (Supplementary Figure 3.17B).

In light of the extensive CMV promoter silencing observed in the process of stable cell line generation, we modified our regulatory systems and used the EF1α promoter to drive the expression of the target transgene and ribozyme switch devices

(Figure 3.2A). The EF1α promoter is weaker than the CMV promoter, but it has also been reported to have more stable long-term expression capabilities[21]. As presented in this chapter, the modified system is sufficiently robust to generate effective T-cell proliferation control systems in CTLL-2 cells.

**Supplementary Text 3.3**

**Controlling for Toxicity and Non-specific Effects of Nucleofection and Small-Molecule Ligand Inputs on Growth and Gene Expression.** Gene expression can be sensitive to a myriad of external factors, and accurate characterization of phenotypic responses, such as cell growth and viability, requires appropriate controls to account for potential non-specific effects of experimental procedures applied to the cells. In particular, the toxicity and other non-specific effects of transfection and small-molecule ligand addition were of concern in the characterization of the ligand-responsive, ribozyme-based regulatory systems described here. Careful controls were included in the experiments reported in this study to ensure accurate accounting of any potential non-specific effects.

Like most T cell lines, CTLL-2 cells cannot be effectively transfected by lipid-based transfection reagents. Therefore, electroporation with Amaxa Nucleofector technology is the method of choice for transfecting CTLL-2 cells. The trauma of nucleofection results in high cell mortality and affects the health of surviving cells. To account for the toxicity of nucleofection, all experiments conducted in this study included as a positive control cells nucleofected with a similar DNA construct harboring an inactive, scrambled ribozyme that lacks an attached aptamer. This control construct has

no ribozyme-based knockdown activity and no ligand-responsive cleavage activity, and it represents the maximum possible expression level from the regulatory system. Viability and fluorescence data from all other samples were reported relative to those of the positive control treated with the same concentration of small-molecule ligand. It has been verified by multiple nucleofection experiments that nucleofection toxicities from similar DNA constructs purified in the identical manner are similar.

The reproducible agreement between two characterization methods—viability (a phenotypic response) and fluorescence (a measure of reporter gene expression)—provided further confirmation of ligand-responsive gene-regulatory activity (Figure 3.2, Supplementary Figure 3.1). To verify that growth cytokine withdrawal (and not nucleofection toxicity) is responsible for the decrease in viability levels observed for cells transfected with active ribozyme switch constructs, transfected samples were split into two identical aliquots, one of which was fed with 100 U/ml of exogenous IL-2, a concentration that is sufficient to sustain healthy expansion of CTLL-2 cells during routine culture maintenance. The IL-2-treated samples had significantly higher viability levels compared to identical samples not treated with exogenous IL-2 (Supplementary Figure 3.18A). Furthermore, the inverse correlation between viability and ribozyme switch copy number disappears in the presence of exogenous IL-2, suggesting that the reduced viability at high switch copy numbers is specifically caused by more efficient gene expression knockdown and the resultant cytokine withdrawal in the absence of exogenous IL-2. In contrast, the addition of exogenous IL-2 does not affect fluorescence levels (Supplementary Figure 3.18B). Taken together, these results indicate that the observed variations in viability levels are specific to the regulatory systems.

The toxicity and potential pleiotropic effects of the small-molecule ligands theophylline and tetracycline were also considered (see Appendix 1 for toxicity curves of various small-molecule ligands in CTLL-2 cells). In transient transfection experiments the fluorescence and viability values of all samples were normalized to that of the inactive ribozyme control treated with the same concentration of the small molecule ligand (as described above) to account for non-aptamer-mediated effects of the ligand, as it is assumed that the non-specific effects of the ligand will be similar for the sample and the control. Negative controls, such as cells transfected with vectors that encode either no growth cytokine or a growth cytokine gene coupled to a fully active, non-switch hammerhead ribozyme control (sTRSV), were included in all transient transfection experiments. The relative viability and fluorescence levels from the negative control samples exhibited no response to ligand addition, indicating that the normalization method adequately accounts for the toxicity and pleiotropic effects of the small-molecule ligands (Figure 3.2B, Supplementary Figure 3.1A).

By using the inactive ribozyme as the normalizing control for all switch constructs in all transient transfection studies, we report the regulatory output of the switches relative to the maximum possible expression range. Compared to the more commonly used method of internal normalization, where each switch construct is normalized to its own internal high value, our method has the effect of reducing the apparent dynamic range of each switch. However, the reporting of switch output to a consistent standard control allows for direct and accurate comparison of the various switches, which is important for system development and characterization. The internal normalization method is employed for *in vitro* gene expression assays on stably

integrated cell lines (Figure 3.6B, C, Supplementary Figure 3.4A), because the maximum expression level of each clone is dependent on the integration site, which varies from clone to clone.

In the characterization of cell lines stably expressing the ribozyme switch constructs, a clonal cell line expressing the positive control construct (inactive ribozyme) was included to identify any non-specific effects of theophylline. As an example, an *in vitro* growth assay was performed on clonal cell lines in the presence or absence of 500 μM theophylline. The cell line expressing the inactive ribozyme exhibited a decreased growth rate in the presence of theophylline (Supplementary Figure 3.18C), indicating theophylline toxicity and verifying that the theophylline-induced increase in absolute growth rate observed from clones expressing the active ribozyme switches were not due to any non-specific growth-stimulatory effects of theophylline (Figure 3.6A, Supplementary Figure 3.3). As another example, positive and negative control cell lines were included in the animal studies and no significant theophylline-dependent differences were observed in the *in vivo* growth pattern of cells that either do not express growth cytokines or express the inactive ribozyme control (Figures 3.7A, 3.7C). In contrast, the *in vitro* and *in vivo* growth rates of clonal cell lines expressing functional ribozyme switch systems show increases in absolute growth rate (not normalized to the inactive ribozyme control) in response to theophylline addition (Figures 3.6A, 3.7B, Supplementary Figures 3.3, 3.6). Taken together, these results indicate that the observed T-cell growth behaviors were specific to the ligand-responsive regulatory system.

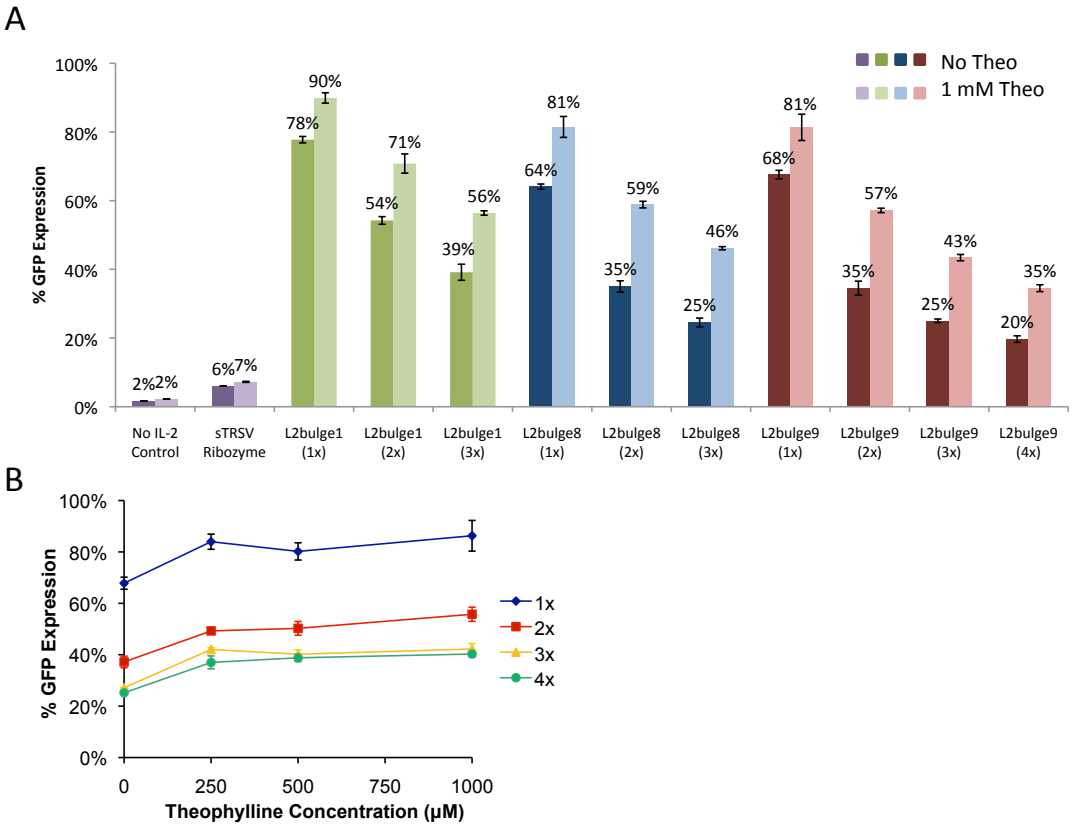


**Supplementary Figure 3.1.** Tunable, small molecule–mediated regulation of gene expression in mammalian cells by ribozyme switches. (A) GFP expression levels are reported for constructs encoding theophylline-responsive switches (L2bulge1, 8, 9) in one (1x), two (2x), three (3x), and four (4x) copies through transient transfections in CTLL-2 cells grown in 0 and 1 mM theophylline. No IL-2 Control, construct not encoding a proliferative cytokine; sTRSV Ribozyme, construct encoding a non-switch hammerhead ribozyme. (B) GFP expression levels are reported for multiple-copy L2bulge9 regulatory systems at various theophylline concentrations. Fluorescence values were normalized as described in Figure 3.2. Values are mean ± s.d. from at least two replicate samples. Fluorescence and viability measurements yielded consistent results, thus validating the use of a fusion transgene as the regulatory target.

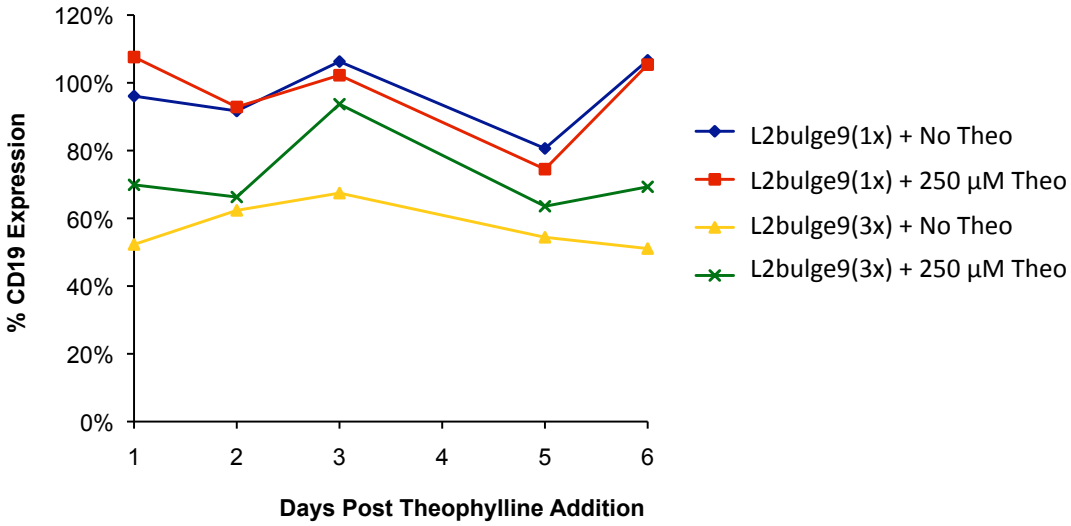


**Supplementary Figure 3.2.** Stable cell lines expressing multiple ribozyme switches exhibit lowered basal level and increased switch dynamic range. Stable integrants were selected by fluorescence-based cell sorting for $CD19^{+}$ populations. Bulk-sorted cells were cultured either with or without 250 µM theophylline for six days and CD19 expression levels were monitored by staining with PE-conjugated CD19 antibodies. Although bulk cell lines stably expressing the single-copy ribozyme switch system did not exhibit significant increases in gene expression in response to 250 µM theophylline, individual clones that exhibited low basal expression levels and significant theophylline-responsive increases in expression were successfully isolated from this bulk population (see Supplementary Figure 3.3).

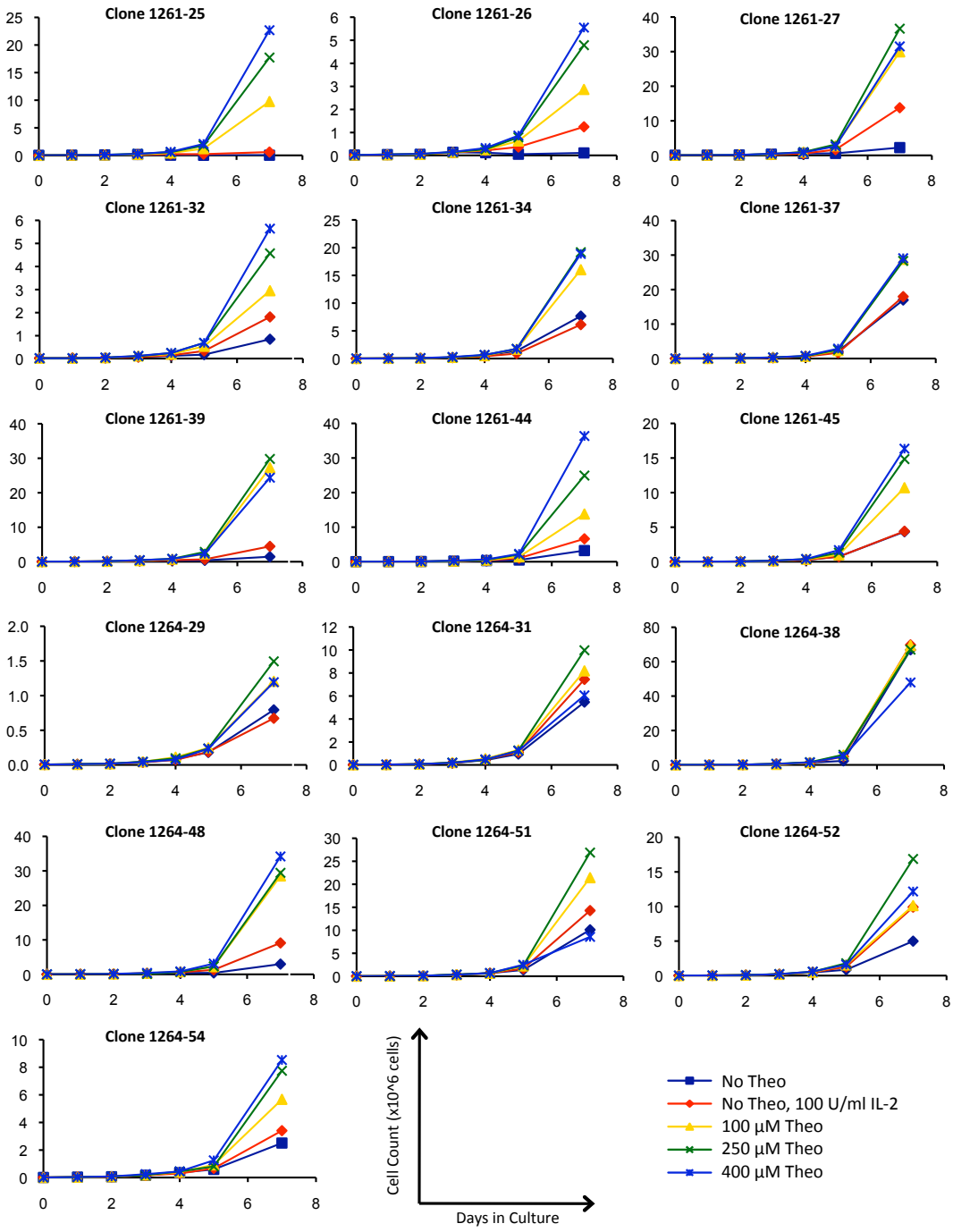


**Supplementary Figure 3.3.** Clonal CTLL-2 cell lines stably expressing engineered ribozyme switch systems exhibit effective theophylline-responsive growth regulation. The cell lines were cultured at various theophylline concentrations, and cell growth was monitored by counting viable cells. Clones indicated as 1261-xx stably express *cd19-tk-il15*-L2bulge9(1x). Clone 1264-xx stably expresses *cd19-tk-il15*-L2bulge9(3x). Growth behaviors differ from clone to clone, as would be expected from non-site-specific integration of the transgene into the host chromosomes. Theophylline-responsive increase in cell growth is evident in 15 of the 16 tested clones, and the growth enhancement is statistically significant for the sample set ($P$ = 0.0150, 0.0011, 0.0013 for 100 µM, 250 µM, and 400 µM, respectively, by Whitney-Mann U test).

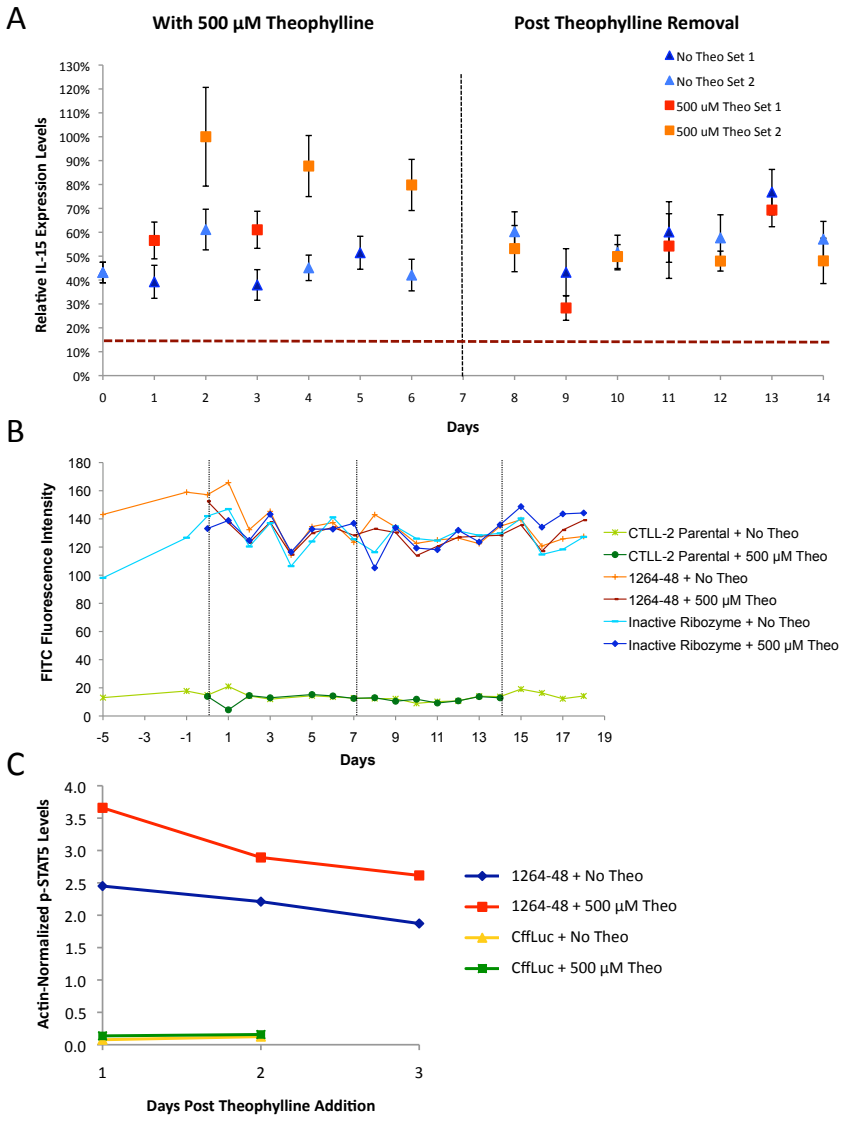


**Supplementary Figure 3.4.** Cells stably expressing the T-cell proliferation regulatory system exhibit theophylline-responsive increases in IL-15 transcription and signal transduction through the JAK-STAT pathway. (A) Relative IL-15 mRNA levels are elevated in the presence of theophylline and return to basal levels upon theophylline removal. qRT-PCR was performed on mRNA extracted from a CTLL-2 cell line stably expressing *cd19-tk-il15*-L2bulge9(3x) (clone 1264-48). IL-15 expression levels were normalized to expression levels of the housekeeping gene *hprt1*, and relative IL-15 expression levels were obtained by normalizing to the inactive ribozyme control. The highest expression level was set to 100%. Reported values are mean ± s.d. from three replicate samples. Samples shown in this figure were collected from the same cultures as described in Figure 3.6B. Red dashed line indicates background signal from a cell line without a CD19 expression construct. (B) Staining with FITC-conjugated IL-15 antibodies shows no ribozyme-mediated knockdown of intracellular IL-15 protein levels. (C) Western blot analysis was performed on protein extracts from CTLL-2 cell lines for p-STAT5. p-STAT5 levels were normalized to that of β-actin. The 1264-48 cell line, which stably expresses *cd19-tk-il15*-L2bulge9(3x), shows increased p-STAT levels in response to theophylline, indicating an increase in IL-15 signaling. The CffLuc cell line, which lacks the ribozyme switch system, serves as a negative control and verifies that theophylline does not nonspecifically activate the JAK-STAT pathway. The CffLuc cell line cannot survive beyond two days without exogenous IL-2, further demonstrating that autocrine growth cytokine production is necessary for sustaining CTLL-2 survival and proliferation in the absence of exogenous cytokine supplies.

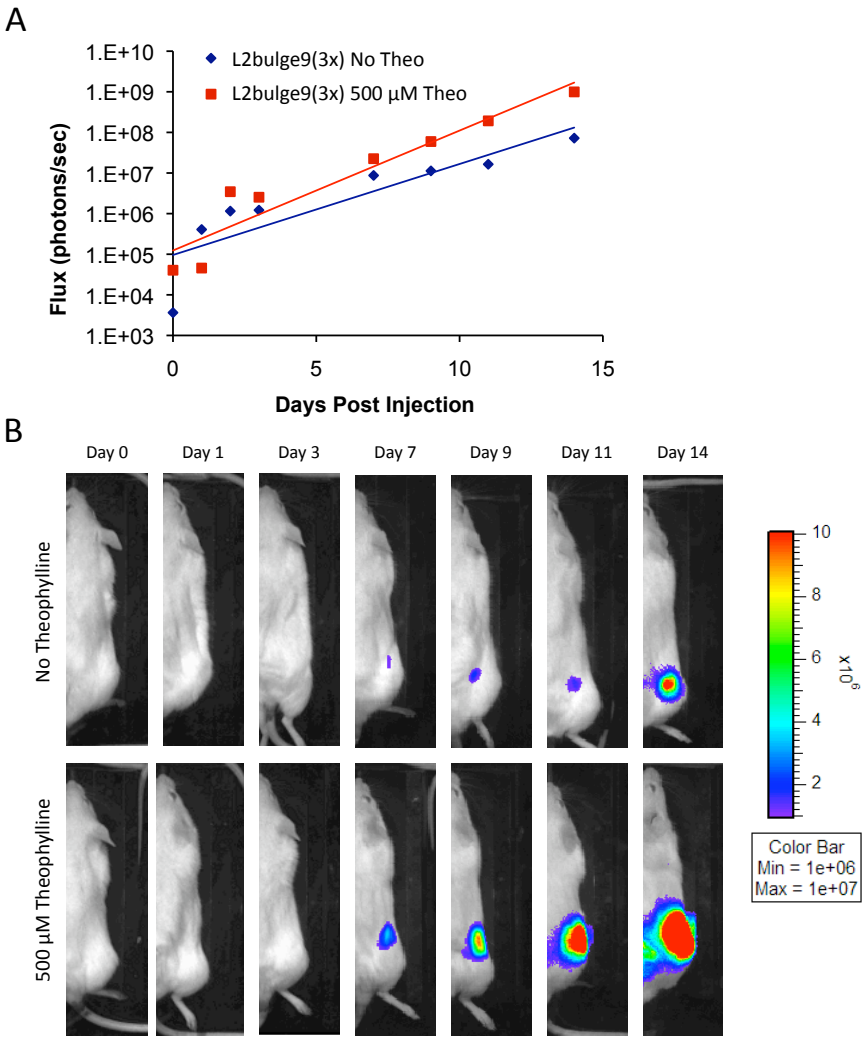


**Supplementary Figure 3.5.** The clonal cell line 1264-48 exhibits accelerated T-cell proliferation in response to small-molecule input. (A) Total luciferase signal flux measurements collected over a 14-day period were fitted to exponential curves and used to calculate the *in vivo* growth rates of injected cells. (B) Images of clone 1264-48 over time. The day of imaging after injection of the stable cell line is indicated.

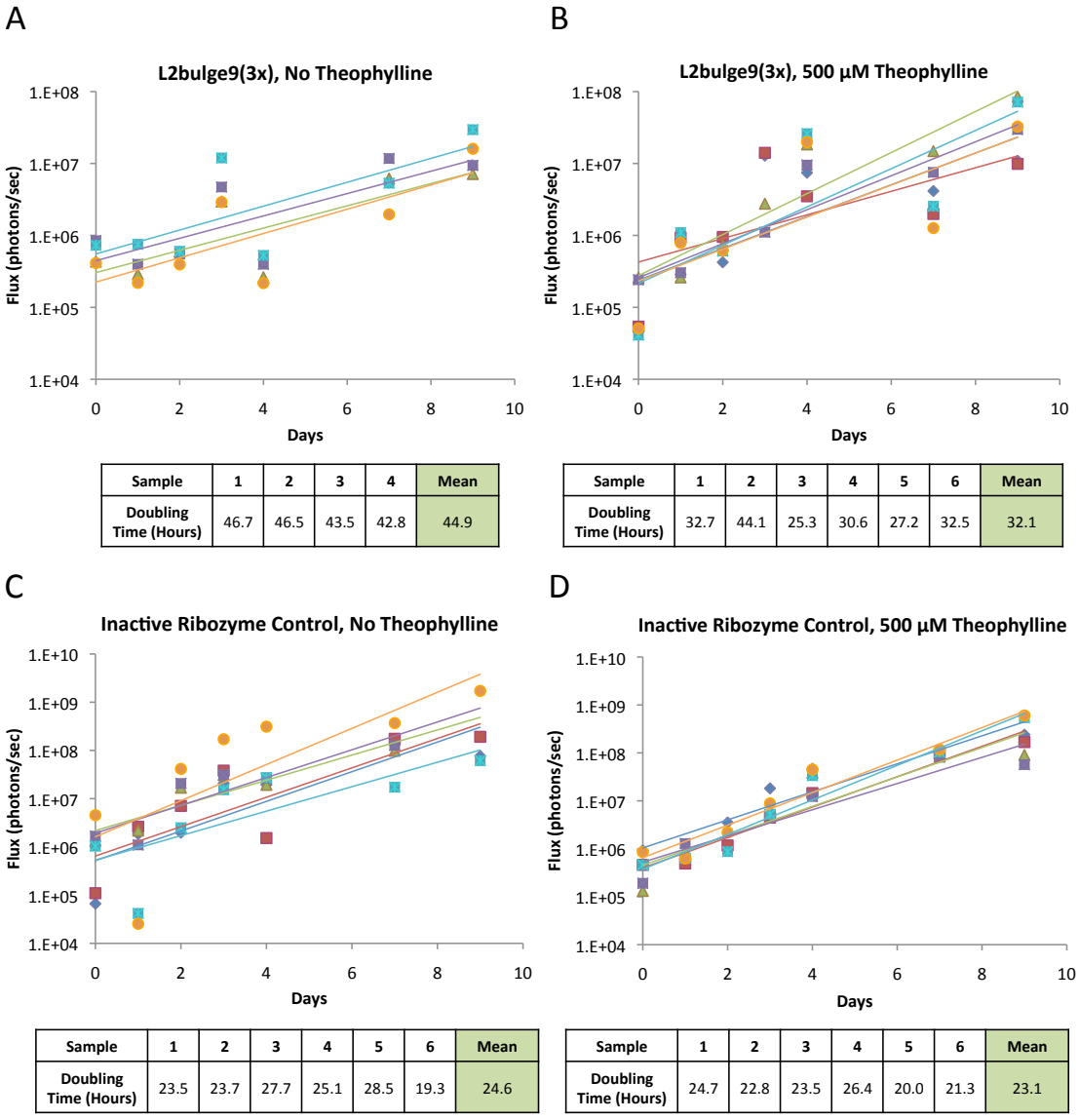


| Sample | 1 | 2 | 3 | 4 | Mean |
|---|---|---|---|---|---|
| Doubling Time (Hours) | 46.7 | 46.5 | 43.5 | 42.8 | 44.9 |

| Sample | 1 | 2 | 3 | 4 | 5 | 6 | Mean |
|---|---|---|---|---|---|---|---|
| Doubling Time (Hours) | 32.7 | 44.1 | 25.3 | 30.6 | 27.2 | 32.5 | 32.1 |

| Sample | 1 | 2 | 3 | 4 | 5 | 6 | Mean |
|---|---|---|---|---|---|---|---|
| Doubling Time (Hours) | 23.5 | 23.7 | 27.7 | 25.1 | 28.5 | 19.3 | 24.6 |

| Sample | 1 | 2 | 3 | 4 | 5 | 6 | Mean |
|---|---|---|---|---|---|---|---|
| Doubling Time (Hours) | 24.7 | 22.8 | 23.5 | 26.4 | 20.0 | 21.3 | 23.1 |

**Supplementary Figure 3.6.** A clonal cell line stably expressing a functional ribozyme-based regulatory system exhibits theophylline-responsive increases in *in vivo* growth rate. Total luciferase signal flux measurements collected over a 9-day period from replicate mice were fitted to exponential curves and used to calculate the *in vivo* growth rate of the injected cells. (A, B) Clone 1264-48 injected in the absence (A) or presence (B) of 500 µM theophylline. (C, D) Inactive ribozyme control cells injected in the absence (C) or presence (D) of 500 µM theophylline. Results indicate a 40% increase in the growth rate of clone 1264-48 in response to 500 µM theophylline and no statistically significant difference in the growth rate of the inactive ribozyme control in the presence and absence of theophylline.

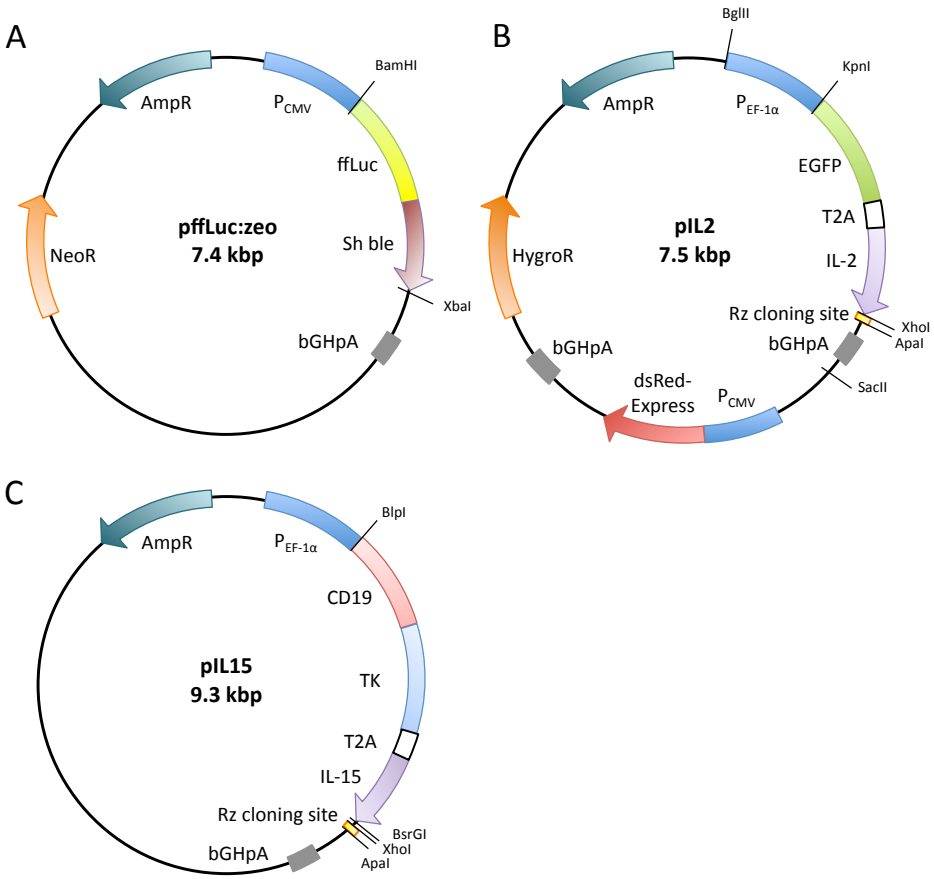


**Supplementary Figure 3.7.** Plasmid maps of T-cell proliferation constructs. (A) pffLuc:zeo was used in generating T cell lines stably expressing firefly luciferase for *in vivo* imaging; (B, C) pIL2 and pIL15 are the base T-cell proliferation expression constructs into which the ribozyme-based regulatory devices are inserted.

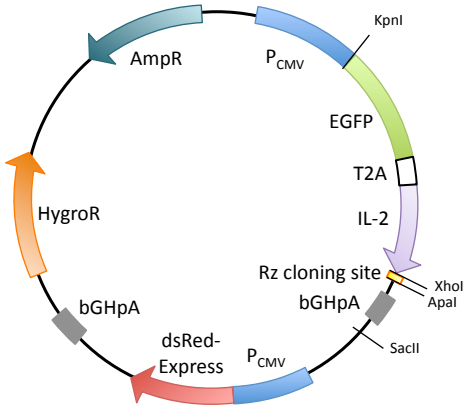


**Supplementary Figure 3.8.** Plasmid map of T-cell proliferation constructs expressed from a CMV promoter. One CMV promoter drives the expression of the regulatory target transgene, *egfp-t2a-il2*, with ribozyme switch devices inserted in the transgene's 3' UTR. A second CMV promoter drives the expression of *dsred-express*, which serves as a transfection marker. The plasmid also encodes for hygromycin resistance, which allows for antibiotic-based selection of stable integrants.

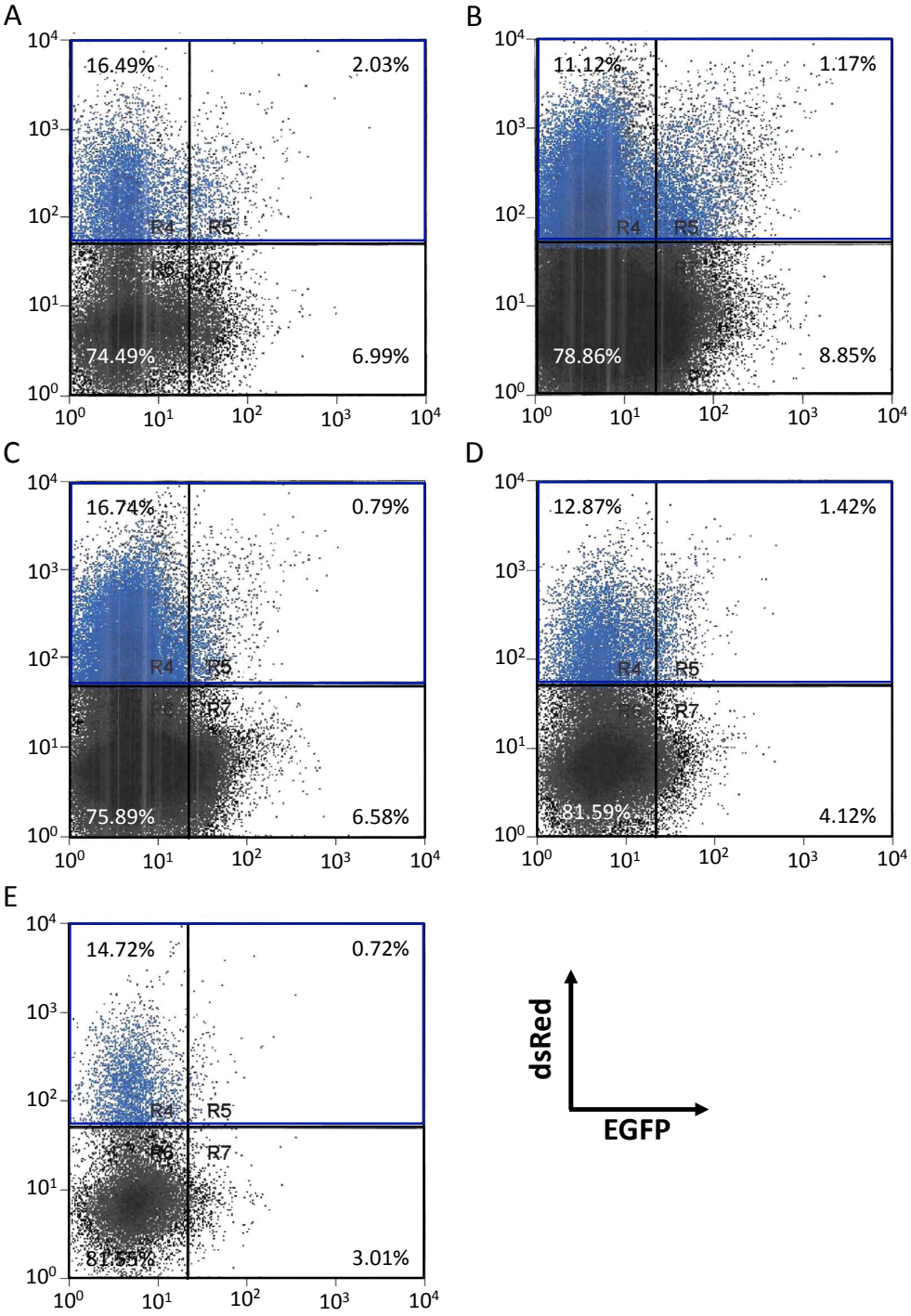


**Supplementary Figure 3.9.** Stable integrants show partial integration and/or CMV promoter silencing. Cells transfected with constructs based on the plasmid shown in Supplementary Figure 3.8 were analyzed and sorted by FACS 19 days after electroporation. All five cell lines showed significant single-positive populations prior to the sort, indicating that one of the two CMV promoters in the construct was either not integrated into the genome or silenced after integration. FACS data are shown for (A) inactive ribozyme control, (B) L2bulge9(1x), (C) L2bulge9(2x), (D) L2bulge9(3x), and (E) L2bulge9(4x). Percentages shown indicate population distribution in the four quadrants delineated by black lines. The blue gate marks the collection window; blue data points indicate collected dsRed$^{+}$ cells.

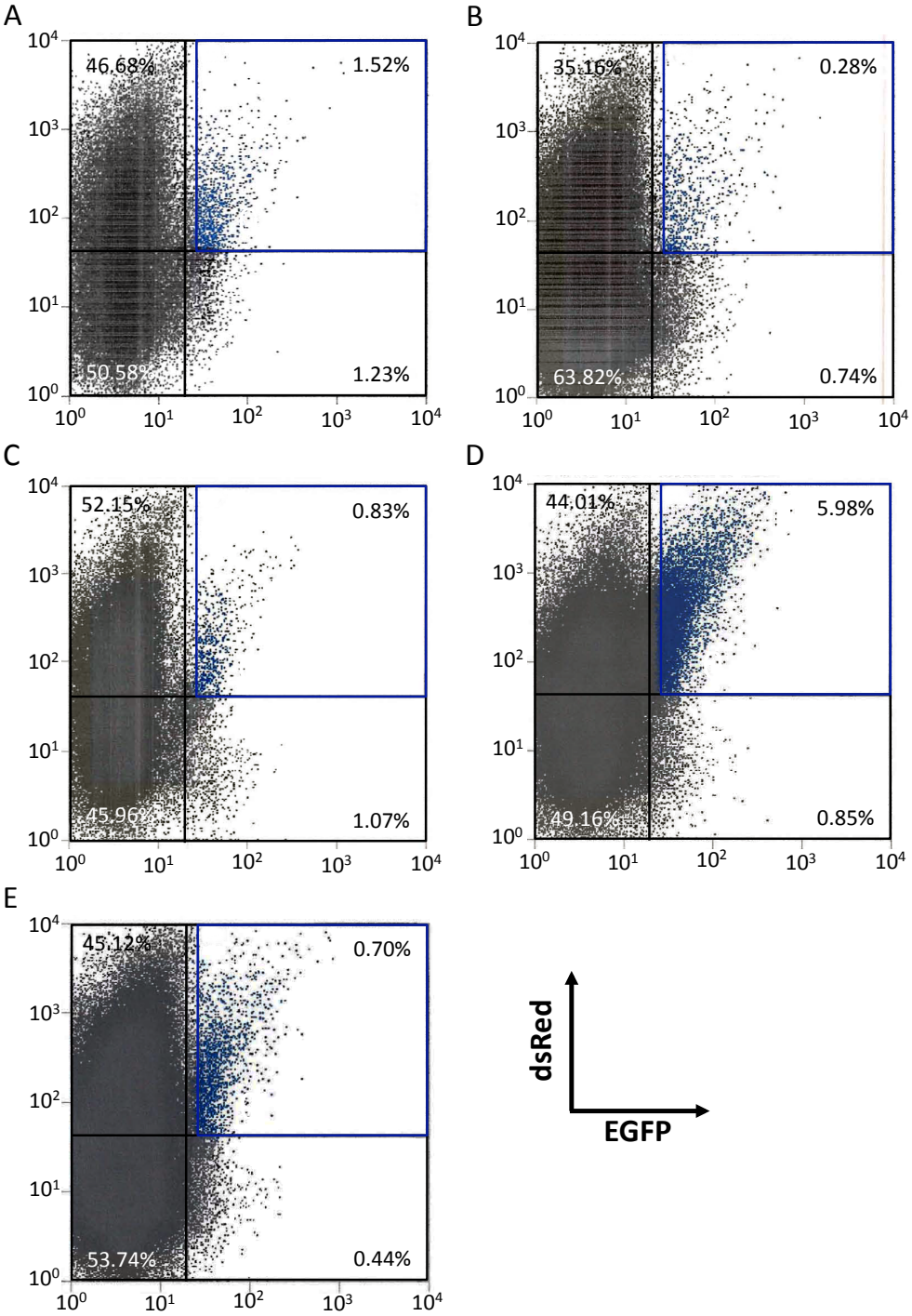


**Supplementary Figure 3.10.** Sorted stable integrants show CMV promoter silencing. Cells previously sorted for dsRed$^{+}$ expression were analyzed and sorted again by FACS 38 days after electroporation. All five cell lines showed significant dsRed$^{-}$ populations, indicating extensive CMV promoter silencing since the first sort. FACS data are shown for (A) inactive ribozyme control, (B) L2bulge9(1x), (C) L2bulge9(2x), (D) L2bulge9(3x), and (E) L2bulge9(4x). Percentages shown indicate population distribution in the four quadrants delineated by black lines. The blue gate marks the collection window; blue data points indicate collected dsRed$^{+}$/EGFP$^{+}$ cells.

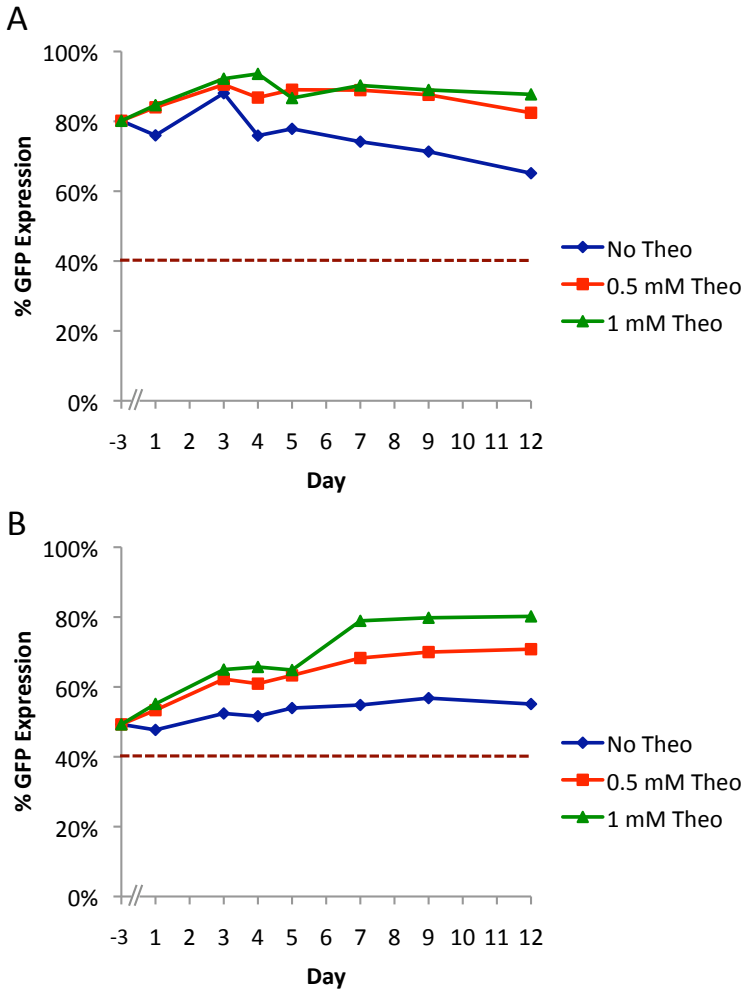


**Supplementary Figure 3.11.** Bulk cell lines stably expressing ribozyme switch systems exhibit gene expression regulation in response to small-molecule input. CTLL-2 cells stably expressing (A) two copies or (B) four copies of the theophylline-responsive L2bulge9 switch demonstrate rapid, dose-dependent upregulation of gene expression in response to theophylline addition. Red dashed line indicates background autofluorescence level of a cell line that does not express GFP (CffLuc).

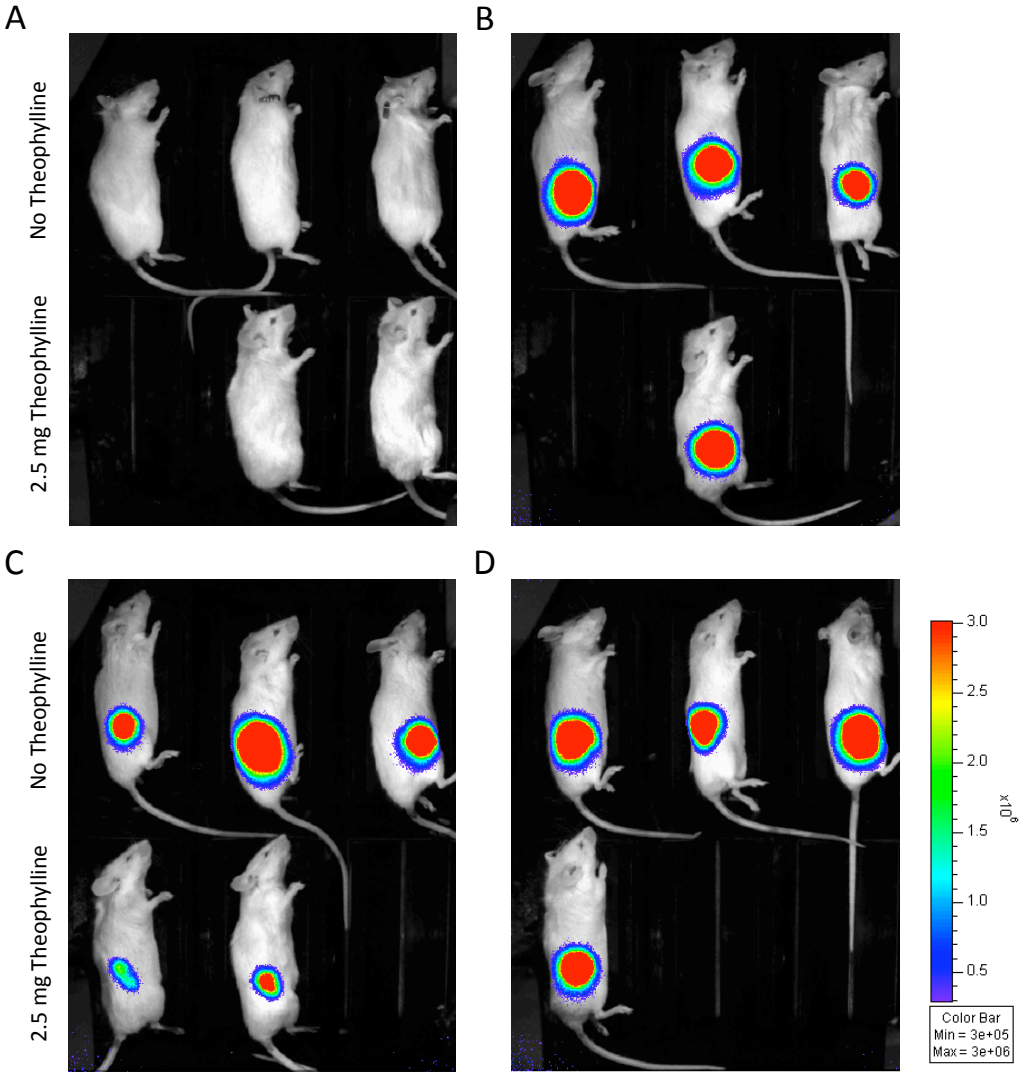


**Supplementary Figure 3.12.** Bulk cell lines stably expressing ribozyme switch systems show excessively high basal growth levels *in vivo*. Clonal cell lines were injected into the right flanks of mice and monitored by biophotonic imaging of luciferase signals. Two systemic injections of 2.5 mg theophylline were given to half of the animal subjects on the day of cell injections. Three animals were included for each experimental condition; missing subjects died on the first day, possibly due to theophylline toxicity. Images are shown for day 10 after injection. All cell lines except the negative control showed engraftment *in vivo* regardless of theophylline availability, indicating the OFF-state expression level was too high to prevent T-cell proliferation. Images are shown for the following injected cell lines: (A) CffLuc (no IL-2 negative control), (B) Inactive ribozyme (positive control), (C) L2bulge9(2x), and (D) L2bulge9(4x).

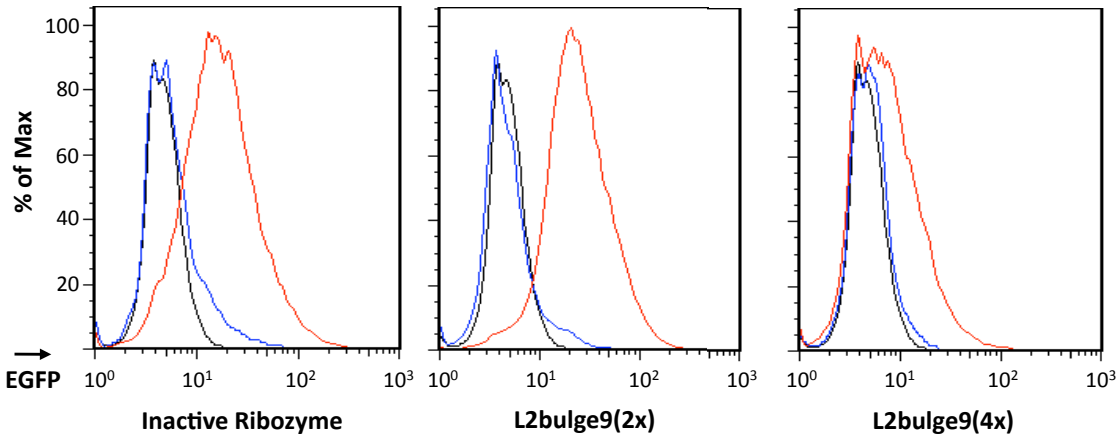


**Supplementary Figure 3.13.** Bulk cell lines stably expressing ribozyme switch systems are selected for high expression levels *in vivo*. Engrafted tumors were excised from the animal subjects shown in Supplementary Figure 3.12. Extracted tumor cells were analyzed for EGFP expression by flow cytometry and showed elevated expression levels compared to corresponding cell lines that had been continuously cultured *ex vivo*. Black, CffLuc (negative control); blue, *ex vivo* cultured cells; red, extracted tumor cells.

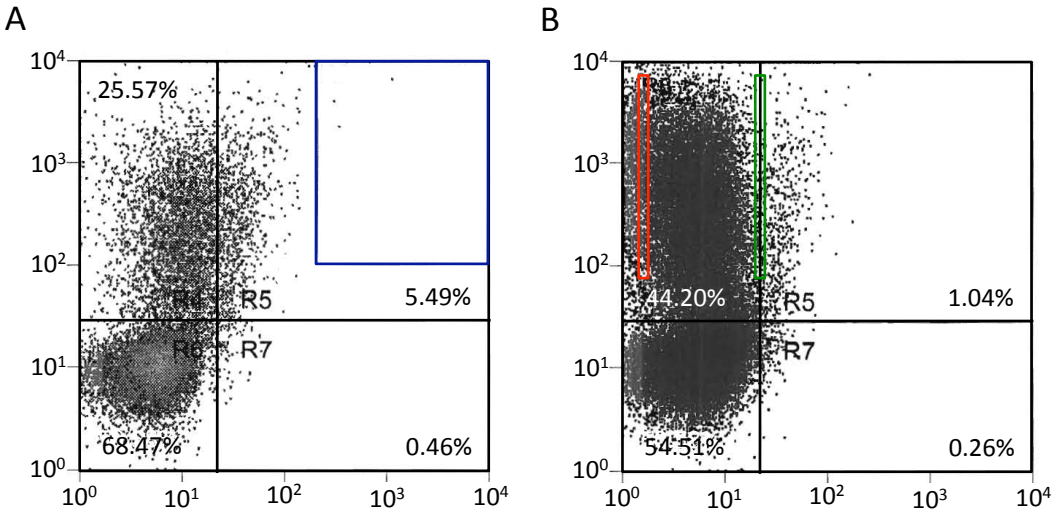


**Supplementary Figure 3.14.** Sorted stable integrants show continuous CMV promoter silencing. Cells previously sorted for dsRed$^{+}$/EGFP$^{+}$ expression were analyzed and sorted again by FACS 109 days after electroporation. Cell lines expressing (A) the inactive ribozyme and (B) L2bulge9(4x) both show over 50% dsRed$^{-}$/EGFP$^{-}$ populations, indicating extensive CMV promoter silencing since the previous sort. Percentages shown indicate population distribution in the four quadrants delineated by black lines. The blue gate marks the dsRed$^{+}$/EGFP$^{high}$ collection window for the inactive ribozyme cell line. Red and green gates mark the dsRed$^{+}$/EGFP$^{-}$ and dsRed$^{+}$/EGFP$^{low}$ collection windows, respectively, for the L2bulge9(4x) cell line.

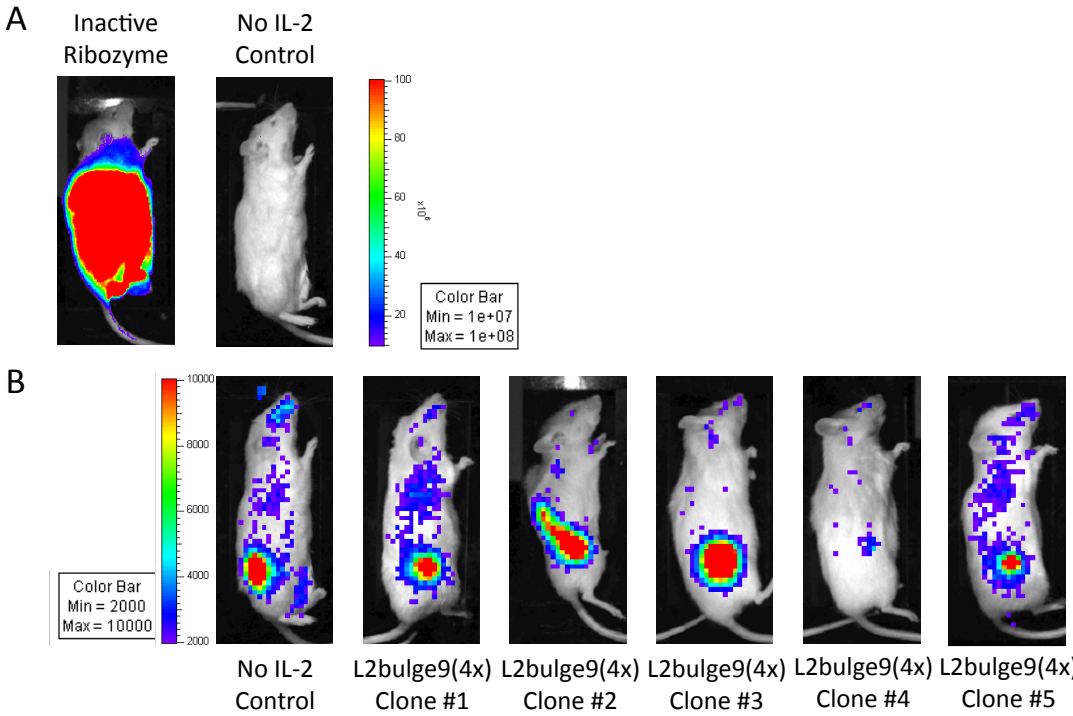


**Supplementary Figure 3.15.** Clonal cell lines stably expressing ribozyme switch systems show stringent OFF-state expression control *in vivo*. Five clonal cell lines expressing L2bulge9(4x) were injected into the right flanks of mice in the absence of theophylline. A clonal cell line expressing an inactive ribozyme and the CffLuc cell line served as the positive and negative (no IL-2) controls, respectively. Images are shown for day 19 after injection. Due to significantly different engraftment and luciferase signal levels between the positive control and the remaining samples, two image settings were used. Signal intensity for each image setting is indicated by the color bars to the side of each panel. (A) Small-binning image for high-intensity samples. (B) Large-binning image for low-intensity samples. The negative control was included in both image settings to allow comparison between groups. None of the L2bulge9(4x) cell lines showed cell expansion beyond background levels, indicating tight expression control in the OFF state .

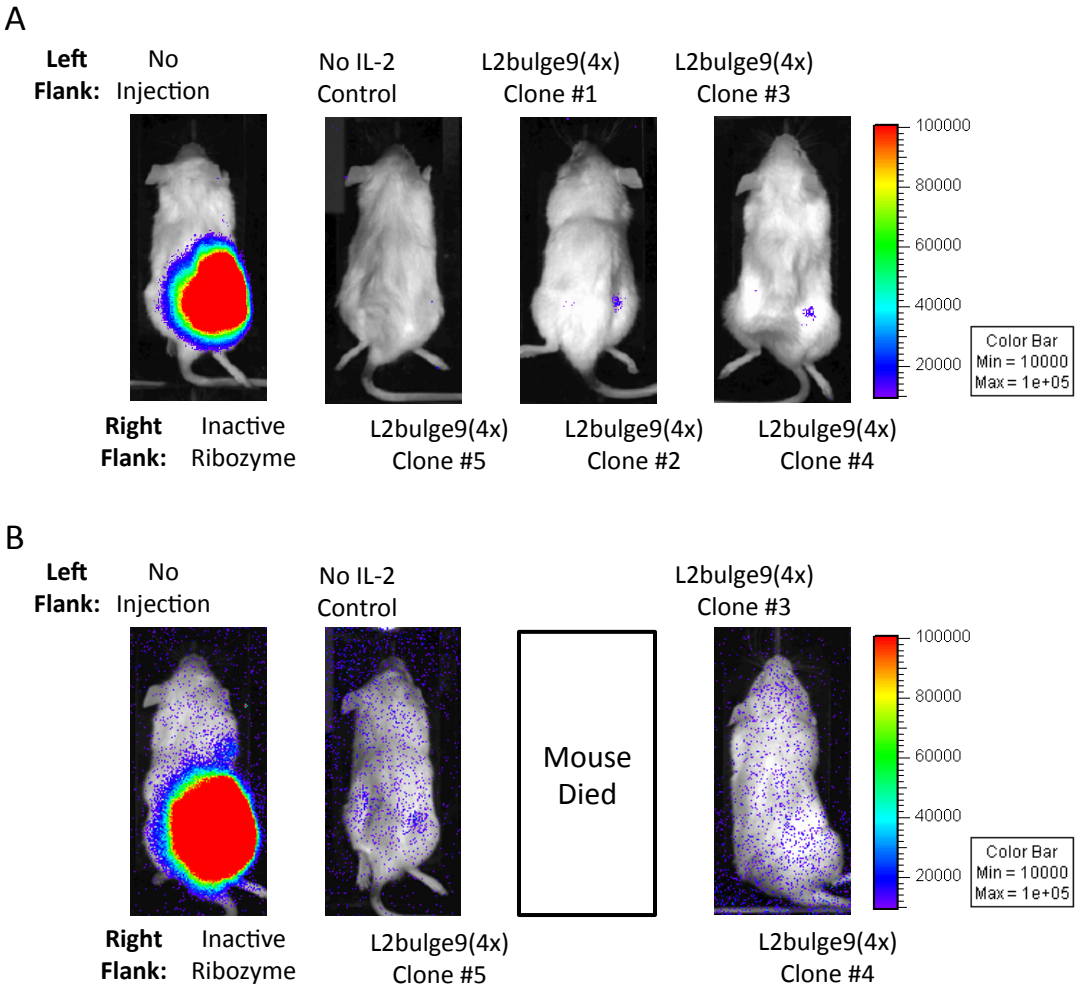


**Supplementary Figure 3.16.** Clonal cell lines stably expressing ribozyme switch systems lack sufficiently high ON-state expression levels to sustain proliferation *in vivo*. Five clonal cell lines expressing L2bulge9(4x) were injected into the flanks of mice in the presence of 200 μM theophylline. A clonal cell line expressing an inactive ribozyme and the CffLuc cell line served as the positive and negative (no IL-2) controls, respectively. Images are shown for (A) day 4 and (B) day 8 after injection. Mice in the same figure panel were imaged simultaneously. Noise seen in panel B is the effect of signal saturation from the inactive ribozyme control sample.

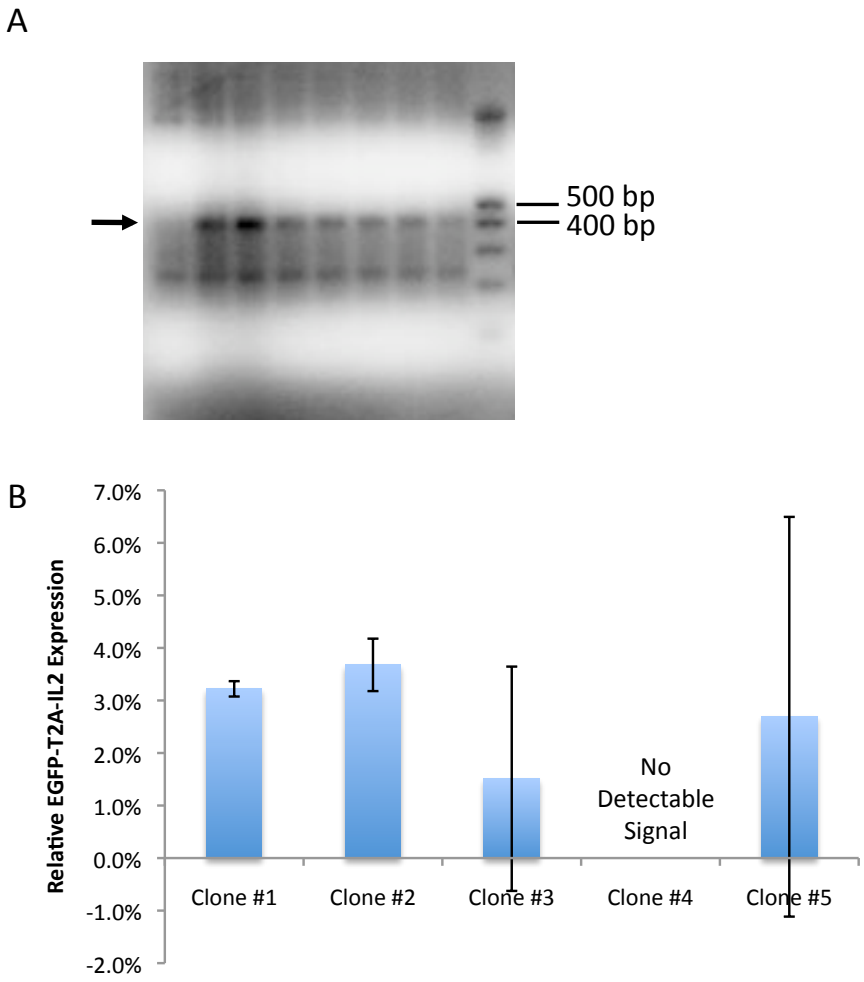


**Supplementary Figure 3.17.** The *egfp-t2a-il2* transgene is stably integrated but expressed at low levels in clonal cell lines. (A) Genomic PCR confirms stable integration of the *egfp-t2a-il2* transgene in all the clonal cell lines tested in the animal study shown in Supplementary Figure 3.16. Genomic DNA was extracted from clonal cell lines, and PCR reactions using forward and reverse primers that anneal to *egfp* and *il2*, respectively, yielded the expected product band (404 bp; marked by arrow). Lane 1, CffLuc (negative control); lane 2, CTLL-2 cell line stably expressing *egfp-t2a-il2* with no ribozyme device attached; lane 3, inactive ribozyme control; lanes 4–8, L2bulge9(4x) Clone #1-#5; lane 9, 100 bp DNA ladder. (B) Clonal cell lines stably integrated with ribozyme switch systems show low EGFP-T2A-IL2 mRNA levels. qRT-PCR was performed on total RNA extracted from clonal cell lines. EGFP-T2A-IL2 expression levels were normalized to expression levels of the housekeeping gene *gapdh*, and relative EGFP-T2A-IL2 expression levels were obtained by normalizing to the inactive ribozyme control. Reported values are mean ± s.d. from duplicate samples.

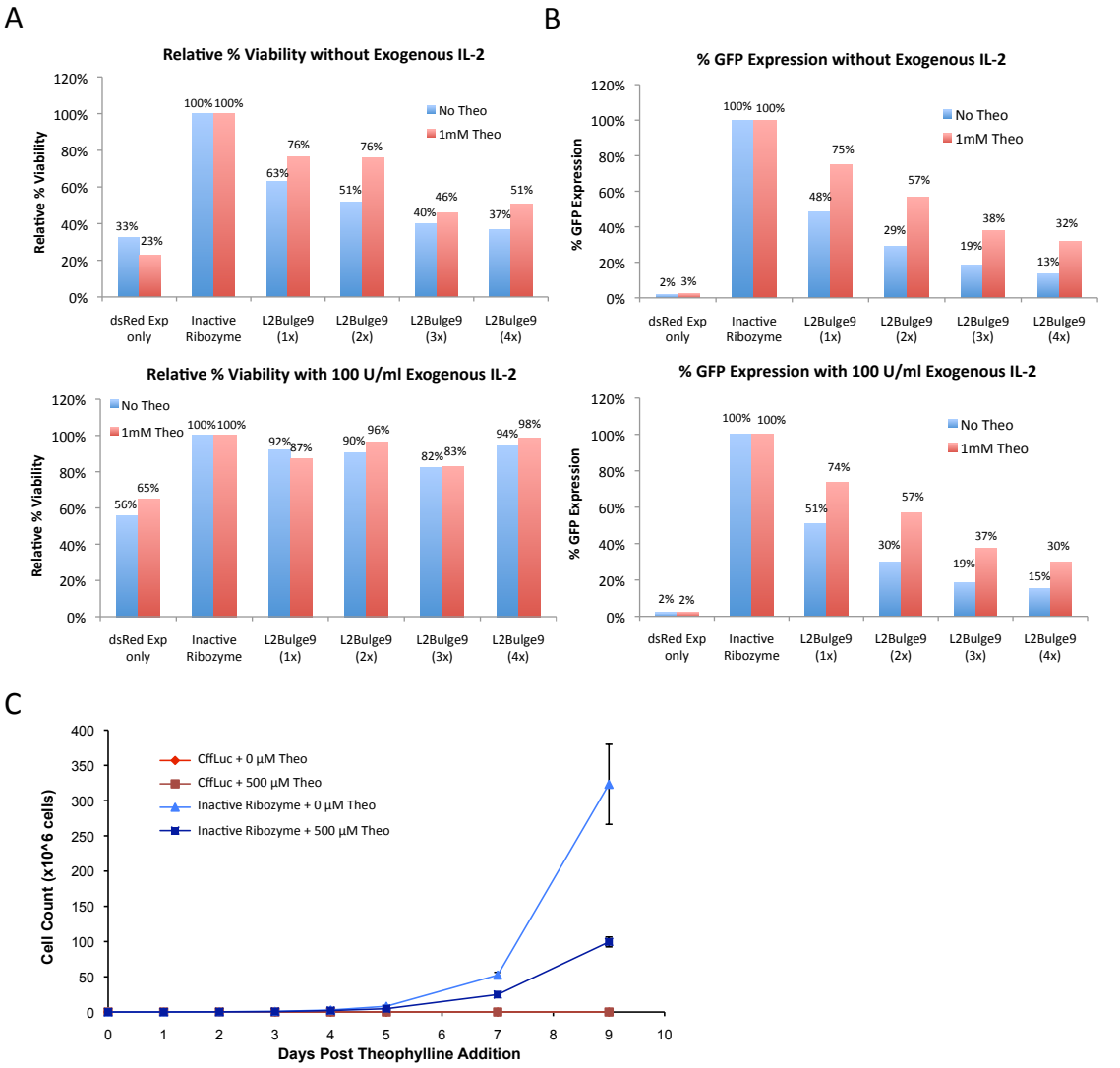


**Supplementary Figure 3.18.** Appropriate controls confirm that observed ligand-responsive switch activities are due to specific effects of cytokine withdrawal. (A) Relative viability of CTLL-2 cells transiently transfected with ribozyme-based regulatory systems as measured by flow cytometry. The presence of exogenous IL-2 elevates viability in all samples and abolishes the inverse correlation between viability and ribozyme switch copy number observed in the absence of exogenous IL-2. These results suggests that the reduced viability at high switch copy numbers observed in the absence of exogenous IL-2 is specifically caused by more efficient knockdown of the cytokine transgene encoded by the regulatory system and the resultant cytokine withdrawal. (B) GFP expression in CTLL-2 cells transiently transfected with ribozyme-based regulatory systems. Fluorescence values were normalized as described in Figure 3.2. The samples shown here correspond to those shown in (A). In contrast to viability behaviors shown in (A), switch activity as measured by fluorescence is unaffected by the presence of exogenous IL-2, indicating that the gene expression modulation is specific to the regulatory system. (C) Theophylline inhibits growth in CTLL-2 cells. CffLuc cells and a clonal cell line stably expressing the inactive ribozyme were cultured in the presence or absence of 500 µM theophylline without exogenous IL-2. Cell count was monitored for nine days by flow cytometry. CffLuc cells failed to expand due to lack of growth cytokines. The inactive ribozyme control, which expresses high levels of cytokine independent of theophylline, showed reduced growth in the presence of theophylline, indicating theophylline toxicity.